Stochastic Ratchets and Cell Junction Shrinkage

Misha Gupta

A dissertation to be submitted for the partial fulfillment of BS-MS dual degree in Science

Certificate of Examination

This is to certify that the dissertation titled "Stochastic Ratchets and Cell Junction Shrinkage" submitted by Ms. Misha Gupta (Reg. No. MS15020) for the partial fulfilment of BS-MS dual degree programme of the Institute, has been examined by the thesis committee duly appointed by the Institute. The committee finds the work done by the candidate satisfactory and recommends that the report be accepted.

Dr. Sanjeev Kumar   Dr. Dipanjan Chakraborty   Dr. Abhishek Chaudhuri

(Co-Supervisor)

Dated: June 8, 2020

Declaration

The work in this dissertation has been carried out by me under the guidance of Dr. Abhishek Chaudhuri at the Indian Institute of Science Education and Research Mohali and Dr. Madan Rao at the National Centre for Biological Sciences, Bengaluru.

This work has not been submitted in part or in full for a degree, a diploma, or a fellowship to any other university or institute. Whenever contributions of others are involved, every effort is made to indicate this clearly, with due acknowledgement of collaborative research and discussions. This thesis is a bonafide record of original work done by me and all sources listed within have been detailed in the bibliography.

Misha Gupta

(Candidate)

Dated: June 8, 2020

In my capacity as the supervisor of the candidate's project work, I certify that the above statements by the candidate are true to the best of my knowledge.

Dr. Abhishek Chaudhuri
(Internal-Supervisor)

In my capacity as the supervisor of the candidate's project work, I certify that the above statements by the candidate are true to the best of my knowledge.

Prof. Madan Rao
(External-Supervisor)

Acknowledgements

I wish to express my sincere appreciation to my supervisors, Prof Madan Rao (National Center for Biological Sciences, Bangalore) and Dr. Abhishek Chaudhuri (IISER Mohali) without whose insights, teachings and ideas, this project would never have reached the stage that it has. I would especially like to thank Dr. Chaudhuri for all his mentorship, guidance and support through the last five years. It has been instrumental in my growth as a person, as well as student of physics. I am also grateful to Dr. S. Alex Rautu and Mr. Saptarshi Dasgupta for all their help during the conception of this project as well as all other members of the group at NCBS as well as the SCMP Group at IISER Mohali. Lastly, I would like to extend my thanks to members of the thesis evaluation committee for their suggestions and support throughout this process. I would also like to thank IISER Mohali for providing me with the funding, physical resources and a space to carry out my work.

I, and as an extension, this thesis, has been shaped greatly by all the wonderful, amazing people at IISER Mohali, NCBS Bangalore, MPIPKS, Dresden and TIFR Hyderabad that I have the absolute privilege of calling my friends. There are memories and scientific discussions that have shaped me and my thought process in ways that I am extremely grateful for. And while I am a firm believer in the fact that a place is its people, IISER Mohali has been so much more than that. It has given me a space to explore myself, grow and truly become who I am today. I will carry the memories from the last 5 years with me for the rest of my life. And in any acknowledgement section of any work, I would be remiss in not mentioning the messenger group of school friends that has annoyed me into sanity for the last 7 years.

None of this would have been possible without the support of my family. I have been blessed with grandparents, uncles and aunts that have always built me up with their unwavering faith in me. I have been blessed with a sister who inspires me. But my greatest strength lies in the support from my parents who have been my anchor and the wind beneath my wings. Amma, Papa, Ena; this is all for and because of you.

Misha Gupta

List of Figures

Notation

f Ratio of time for which pulse is off and on in toy model

L Length of the junction being modelled as a spring

τ_m Time Period of the myosin pulse in later models

L_0 Rest Length of Spring

τ_c Time Period of the E-Cadherin pulse in later models

F^α Active Contractile Force on the junction

τ Coefficient after non-dimensionalisation of dynamic equations

F   Free Energy of the System

W   Thermodynamic Work Done on the system

$\Delta\tau$ Time difference between myosin and E-Cadherin pulse

a.u   Arbitary Units

γ Damping Term

B Elastic Coefficient for Spring

$\mathcal{A}$ Amplitude of Active Force

S_i, i = 1,2   Slope of two movements in the structure of L_0 in toy model, corresponding to aggregation and fragmentation of Cadherin Clusters

$\mathcal{Q}$ Offset in L_0 caused by E-Cadherin turnover

Contents

Chapter 1

What are Biological Ratchets?

A ratchet is essentially a device permitting only unidirectional motion. Movement or changes happen in irreversible steps. However, this ratchet cannot exist in an isotropic medium, even in the presence of brownian noise. Structural features alone cannot bias Brownian motion to create a ratchet.[1] This has been illustrated by Feynman in [16] using a toothed gear and a weather vane. In an isotropic medium with Brownian noise, there will be no net motion averaged over time as any forward motion will cancel out any backward motion. A gradient of some sort or an anisotropy to drive the ratchet (usually created by external active forces in most biological systems) is needed to produce net unidirectional motion and do work. This has been also been illustrated by Feynman with the help of a toothed gear and a pawl.
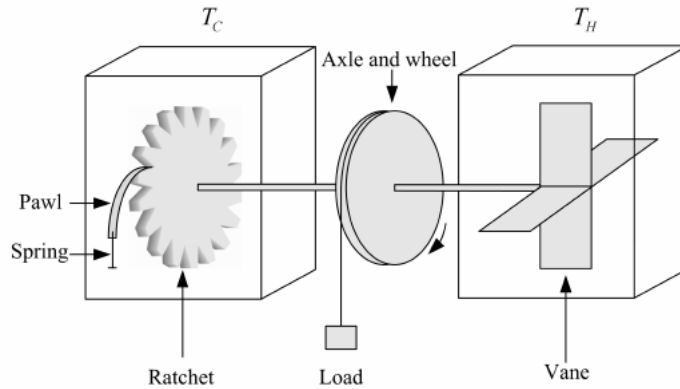
Figure 1.1: Ratchet and Pawl, as taken from Feynman [16]

Here, the device is set up as a weather vane in a box of gas particles at a temperature T_H. The toothed gear is connected to a pawl in a box with gas particles at a temperature T_C. They are connected by an axle and a wheel with a load which can be used to measure work done, if any. We set up a thermal gradient by $T_H > T_C$. In the T_H box, the gas particles randomly bombard the weather wane, causing it to 'jiggle' and move the connected gear in both, forward and backward, directions. This bombardment is random and Brownian in nature and we expect there to be no net motion in a given direction. However, the pawl prevents the backward motion in the T_C box and only unidirectional forward motion is allowed. [1]

---

[1] This seemingly causes the second law of thermodynamics to be violated. But we must remember that the second law is statistical in nature and it has been proven that entropy can spontaneously decrease in a system with an exponentially decreasing probability[14],[15].)

Each movement of the teeth in the gear also cause the pawl to 'bounce' when it opposes the backward motion. The energy produced in this causes the air around the gear to heat up. As the T_C box heats up, Brownian motion and bombardment occurs here on the pawl too. While the pawl is bouncing around, the tooth can slip even in the backward direction. Hence, at $T_H = T_C$, when the bombardment on the weather vane and the pawl is the same, the motion of the gear is completely random and there is no net movement. Purely equilibrium thermal fluctuations cannot cause a movement current. To cause uni-directional motion, some energy ϵ must be provided to the vane end or the driving end of the ratchet to ensure that $T_H > T_C$ is maintained.

However, even within a ratchet, some amount of backward motion is permitted, often called 'backlash'. This backward motion is heavily energetically penalised. In a long-time limit, the backward motion is negligible (unless there is an external driving force in that direction) and we have effective one-directional motion. This backlash can be used as a potential measure of the quality of the ratchet.

Analogies can easily be drawn between such ratchets and biological active systems. In most biological systems where random diffusion can dominate, ratchet mechanisms are often used to explain unidirectional motion and movement. Notably, most biological ratchets do not use gradients to cause motion but rather non-directional sources of energy like heat or chemical forces.

1.1 Some examples of biological ratchets

1. Molecular Motors in muscles: Molecular motors that depend on ATP consumption for activity often have to contend with thermal noise on comparable orders of magnitude. Despite this, there are very few backsteps when a motor is carrying a load. However, spontaneous reduction of entropy coupled with phenomena like forward fluctuations cause conformational changes in the substrate and keeps the motor to keep moving forward in a ratchet-like manner.[9]

2. GTP-GEF Cascades in cargo trafficking: Rab GTPase Enzymes are thought to be master regulators for trafficking cargo across the cisternae of golgi in cells. This is a complex molecular mechanism involving SNARE proteins, GEF's (guanine nucleotide exchange factors) and GAP's (GTPase activating proteins). These are often set up as a cascade in a 'ladder' formation and follow the same irreversible ratchet mechanism to facilitate transport across the golgi.[11]

For this thesis, we will be focusing on cellular junction shrinkage while attempting to model it as a ratchet. During tissue morphogenesis and remodelling, inter-cellular junctions must shrink to allow cell shape changes. This has been seen during tissue extension in the *Drosophila* Embryo which is known to be initiated by the active shrinkage of the vertical junctions. Experimentally it has been observed that this shrinkage happens in a ratchet-like manner, with steps being controlled by the density of molecular motors (Myosin II and E-Cadherin clusters) with noisy dynamics at the cell junction.

Chapter 2

Cellular Junction Shrinkage

Any tissue is composed of multiple cells and all of these cells must interact with each other for all physiological processes, ranging from development to having mechanical stability. These interactions often involve 'cell junctions' or 'inter-cellular bridges' which are specialised plasma membranes. Different kinds of such junctions mediate interactions, either between different cells or between the plasma membrane and the extracellular matrix. There are 3 particular types of junctions that can be found between the plasma membrane of neighbouring cells in animal cells.
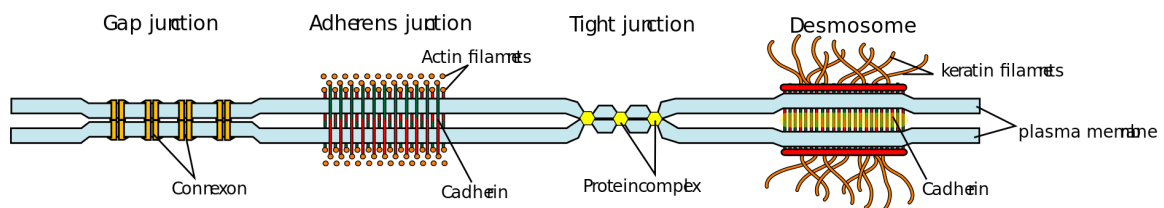
Figure 2.1: Illustrative example of types of cell junctions in animal cells. We focus on the Adherin Junctions. The junction consists of Actin Filaments that extend into the cell as well as Cadherin Proteins that live on the junction itself.
Image Source: Wikipedia (Public Domain)

1. Occluding Junctions or Tight Junctions: These junctions use multi-protein complexes in vertebrates to prevent leakage of fluid across cells. They could either form seals or pathways for 'leakage' of selective material. In invertebrates, an analog is found in the form of "separate" junctions.

2. Communication Junctions or Gap Junctions: These junctions connect the cytoplasm between neighbouring cells. (The analogue in plant cells would be the plasmodesmata) They facilitate electronic, chemical and trans-membrane communication between cells.

3. Anchoring Junctions: They can be of multiple types, Adherin Junctions, Desmosomes, and Hemidesmosomes. Adherin junctions are directly connected to the actin cytoskeleton and composed of various proteins; of which Cadherins (from "calcium-dependent adhesion") are key. Since they are directly connected to the cytoskeleton, the motor protein Myosin also plays a direct role in its dynamics.

We will focus on adherin junctions in this work, and particularly on the dynamics of the cell junctions during the germband extension of *Drosophila* embryo.

3

2.1   A detailed look at cell shrinkage in the *Drosophila* embryo

During early development of *drosophila*, the germ band extension is an important step. The germ band is a primary layer of cells that formed during the embryonic development and eventually develops into the trunk of the embryo. It is seen to almost double in length (along the anterior-posterior or head-tail axis of growth) while narrowing along the perpendicular (dorsal-ventral or side-side) axis.[8]
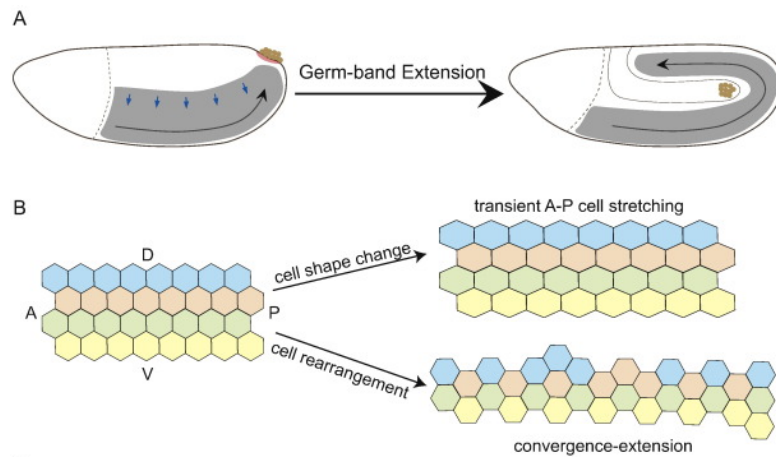
Figure 2.2: A) The germ band, marked in grey, undergoes tissue remodelling to double in length and narrow in shape, eventually folding upon itself and forming the trunk of the embryo. **B)** This extension happens via a process of tissue remodelling where cells undergo shape changes by stretching in one direction (as in this embryo) or by cell rearrangement. [8]

Time Lapse Microscopy on the *Drosophila* embryo has shown this tissue extension happens through changes in neighbouring cell shapes. The changes happen in a manner that maintains the structural integrity of the epithelial tissue and adherin junctions (and often involves cellular intercalation). The tissue gets remodelled when the cellular junctions shrink according to the topological T1-T2-T3 transitions. **Notably, no cell division takes place during this process.** The junctional collapse happens only along the vertical junctions of the cell due to the planarity and polarity in the embryo. The vertical cell junction (red line in Fig. 2.3) must collapse before the junction can extend in the perpendicular direction (blue line in Fig. 2.3).
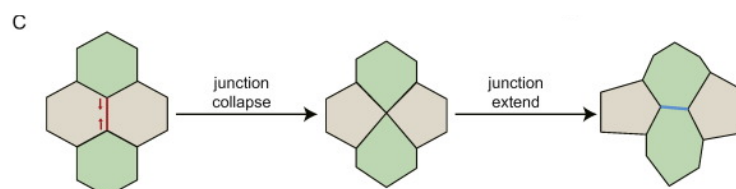
Figure 2.3: In the tissue, initially the grey cells are in contact with each other and the green cells are separated by a cell junction, marked in red (T1). After initiation of shrinkage, this junction collapses and all four cells share a common point of contact (T2). A new cell junction is formed by extension, perpendicular to the original one, marked in blue. The tissue has now extended in length in the horizontal level but narrowed in the vertical direction (remodelled). [8]

2.2 Molecular Ingredients of Shrinkage

It is believed that shrinkage is induced by an interplay of force generators (Myosin II) and force sensors (E-Cadherin). The actin network also plays an important role.

1. The Myosin super-family consists of a large number of ATP-dependent motor proteins with actin-based motility. Consisting of a head, a neck and a tail, these proteins 'walk' along the actin filaments and are capable of carrying cargo that interacts with the tail. Linker proteins form the neck. The head binds to the filament and does the 'walking'. The head also generates force (based on a ATP Hydrolysis fuelled mechanism) during its walk and hence the Myosin is a **Force generator** here. There is a large variety of proteins and isoforms in this super-family. For this thesis, we shall be focusing on the non-muscle, junctional, Myosin-II.

2. Cadherin (from Ca^{2+} Dependant Adhesion) are cell-adhesion molecules that play important roles in Adherin Junctions. The Cadherin super-family consists of a large number of proteins divided into four sub-groups. For this thesis, we shall be focusing on Epithelial Cadherins (E-Cadherin) that belongs to the 'Classical' subfamily. These E-Cadherin exist as various clusters near the junction and within the context of the junctional shrinkage, these are the **Force Sensors**. E-cadherin plays a very important role in cell-cell force transduction and it is strongly coupled with the actomyosin network.
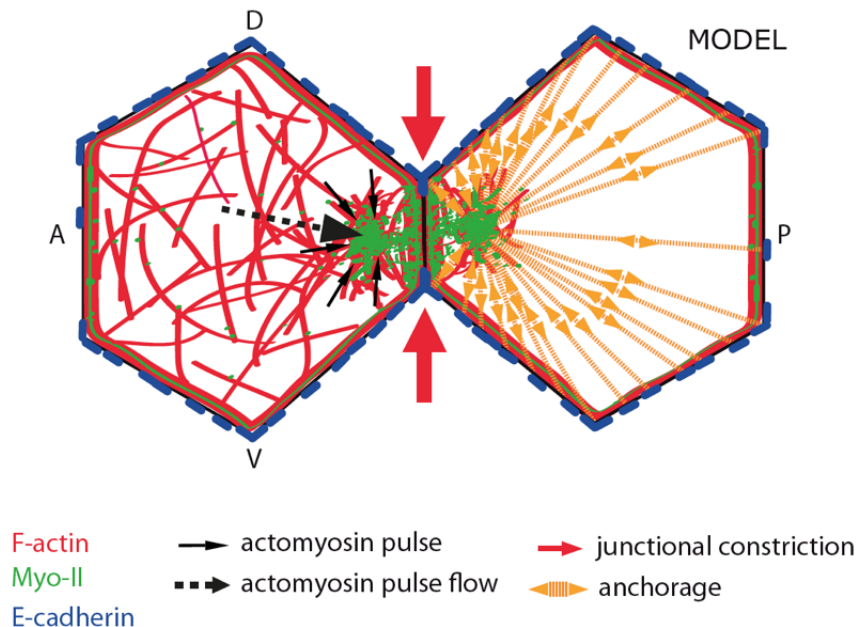
Figure 2.4: Cellular Junction Shrinkage is mediated by Myosin Pulses (marked with black arrows). The Myosin-II protein lives on the F-Actin mesh (marked in red) and gets enriched at the junction during shrinkage. This causes the vertical junction to shrink (marked with the red arrows). This constriction is opposed by Epithelial Cadherin Proteins that live on the membrane (marked in Blue) by redirecting the myosin enrichment.

Junction shrinkage is believed to be driven by the enrichment of Myosin on the junction[8],[13]. Once shrinkage is initiated, a myosin pulse has been observed to periodically enrich the junction with Myo-II. The pulse acts as a force transducter and transmits the tension. The pulse also seems to coincide with the step wise shrinkage. The cell adhesion proteins, mostly Epithelial-Cadherins (E-Cadherins) oppose this shrinkage and hence act as force sensors. E-Cadherin forms different kinds of clusters[6], far from and at the junction. Non-junctional Cadherin clusters stabilise and resist the cortex flow. It is also believed that these clusters resist furrow ingression during cytokinesis[12]. At the junction, the cis and trans E-Cad clusters form, linked to the actin cytoskeleton and respond differently to the myosin pulse. The junction is two lipid bi-layers stuck together. The cis clusters form on the same side the bi-layers and the trans clusters form across the bi-layers, binding to the E-Cad from the neighboring cell. There is constant decay and formation of these monomers, cis and trans clusters. The trans clusters redirect the myo-II away from the junction upon enrichment and oppose the shrinkage.

2.3 The Myosin Driven Ratchet

Experimental work has proven that the Myosin-II driven shrinkage mechanism is indeed a ratchet. The Myosin pulse and the E-Cad response has been experimentally visualised (As seen in [2]).

MyoII-mCherry   E-cadherin-GFP
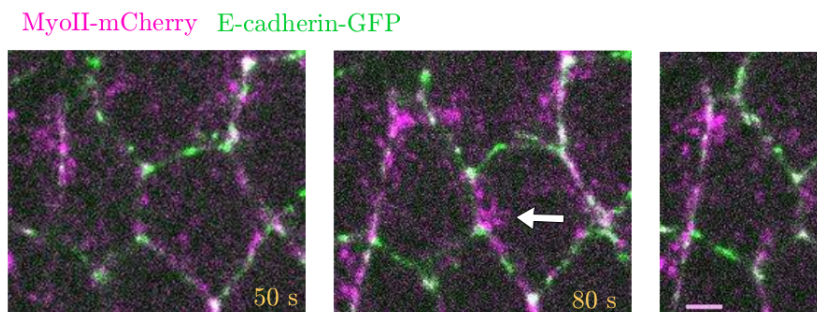
Figure 2.5: Myosin Enrichment at Cell Junction [2]. Each subsequent frame ahead in time. The Myo-II has been marked using the Pink marker and the E-Cad Protein has been marked using the Green marker. We can observe myosin enrichment at the collapsing cell junction(marked by the white arrow).

In the experiment, the Myo-II are tagged by mCherry, a protein marker that fluoresces red/pink when imaged and the E-Cad were tagged by the GFP (Green Fluorescent Protein) which fluoresces green under imaging. The E-Cad is observed all along the cell membrane. As time goes on, periodic enrichment of the cell junction in Myo-II (by a Myosin Pulse) is observed. At each pulse, the length of the cellular junction can be measured.
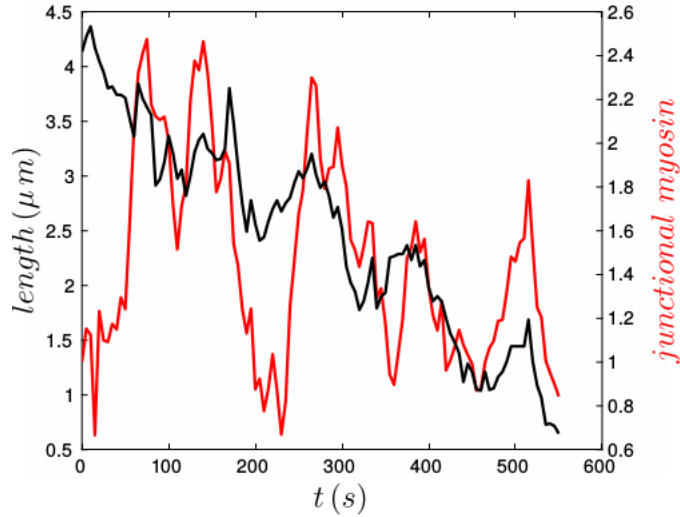
Figure 2.6: Myosin Pulse [13] dynamics with time on the horizontal axis. On the vertical axis, the junctional length is expressed in μm in black. This is overlaid with the Myosin Pulse (independent of the y-axis) in red.

It is observed that the junctional length shrinks down in a step wise manner (with noise due to noisy dynamics of the molecular ingredients). Each step-wise shrinkage coincides directly with a myosin pulse as see in Fig. 2.6. We can reliably conclude that junctional shrinkage happens in a ratchet like irreversible manner and this ratchet is driven by Myosin Pulses and enrichment of Myo-II at the cell junction. To understand this ratchet mechanism in greater detail, we study an already existing microscopic model of the cell junction.

2.4 Microscopic model of the Cell Junction
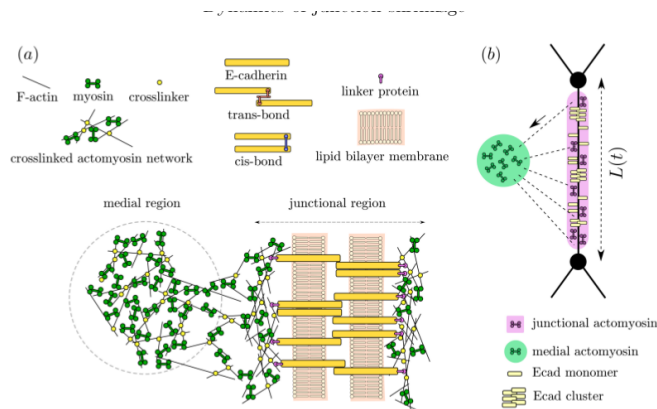
Figure 2.7: Microscopic Model of Cell Junction, as taken from [2]. We focus on junctional myosin (marked in purple) and E-Cad clusters (marked in yellow) tha exist in their trans forms. **A)** The molecular ingredients of the shrinkage mechanism can be seen. It is important to note how the trans E-Cad clusters form bonds extending into the cells across both the lipid bi-layers. **B)** An effective 1-D model of the cellular junction can be seen with a junction length of $L(t)$. This model has been described mathematically in the next section.

The preceeding figure and details of the microscopic model have been taken from [2]. Only the trans-cadherin clusters are actually involved in opposing shrinkage. The real biological junction is a two dimensional object, composed of 2 lipid bi-layers in the horizontal dimension (in plane) and groups of trans and cis E-Cadherin clusters in the vertical (in plane) dimension. Microscopic descriptions using the molecular densities of Myo-II and the E-Cad protein were written down in [2] in full microscopic detail. This can be modelled as an active spring motivated by the spatio-temporal dynamics observed in experiments. The actomyosin network can can be considered a visco-elastic element due to the presence of active stress generators in the form of Myo-II motors. The amount of stress depends on the Myo-II density, the dynamics of which were written down using a basic binding-unbinding model. There is also stress dissipation, in part by the E-Cad molecules. A similar description, using a visco-elastic element with dissipation terms like in a Kelvin-Voight model can also be found in [5]. A hydrodynamic theory for the same was developed in [2] to end up with an effective 1-D model for the junction (Fig 2.7 b). This model has also been proven to capture features of actomyosin pulsation and local contractile forces in [2]. This active spring is characterised by the dynamic variable $L(t)$ - the junction length. The length dynamics were written down as follows:

$$\gamma \dot{L}(t) = -B(L(t) - L_0(t)) - F^\alpha(t) \tag{2.1}$$

Here, γ is the damping coefficient, B is the elastic coefficient for the spring, $L_0(t)$ is the time dependant rest length and F^α is the active contractile force.
Here, the external active force is already known and is strictly speaking, not tunable. The addition of a time dependant rest length $L_0(t)$, motivated by the ratchet like mechanism in shrinkage and explained in section 2.6, makes the equation detailed balance violating. This will be the crux of our model.

2.5   Writing down a coarse grained model

The microscopic details of the model have already been worked out in [2], along with a hydrodynamic description. However, there is merit to writing a more coarse-grained model to try and understand the thermodynamics of a non-equilibrium process to gain a deeper understanding. We take this more coarse grained approach, assume equation 2.1 to govern the junction dynamics and attempt to understand the underlying dynamics of the rest length $L_0(t)$. There are several assumptions that already go into this:

1. The first term is 'restoring force' like. The negative sign accounts for the restoring effect and hence puts a restriction such that $B > 0$

2. The active force $F^\alpha(t)$ is a contractile force based on phenomenology. The negative sign also constrains the magnitude of the force to be positive such that $|F^\alpha(t)| = \mathcal{A} > 0$. There are 2 timescales (when the myosin pulse is on Δt_1 and when the myosin pulse is off Δt_2), and the amplitude of the force $\mathcal{A}$

$$F^\alpha = \mathcal{A} f^\alpha(t) \tag{2.2}$$

Here $f^\alpha(t)$ can take multiple forms. An obvious choice would be a box function like $\text{sgn}(\sin 2ft)$, corrected to having an unequal duty cycle.
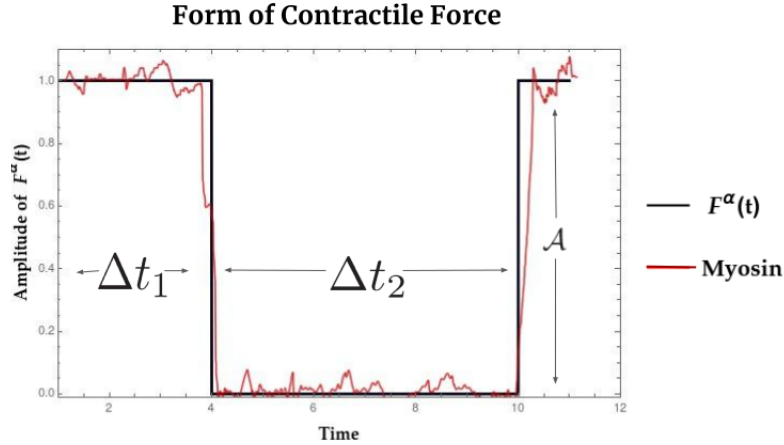
Figure 2.8: Structure of the active force $F^\alpha(t)$. The horizontal axis has time and the vertical axis has the amplitude of the force $\mathcal{A}$ in black, overlaid with the myosin pulse in red (not to scale). The force acts in a pulsatory manner and this pulse continues for the duration of shrinkage. The pulse is on for Δt_1 and off for Δt_2

The key point is that when the pulse is on, the force generated by the Myosin Motors acts on the junction to try and shrink it. We make the natural assumption that the active force is affected only by the myosin dynamics.

3. Actual myosin dynamics are very noisy. However, we work in the deterministic limit for mathematical tractability.

2.6   Where is the Ratchet?

Experimentally, we have no access to any dynamics of the rest length of the spring which we assume to be time-dependent. Hence, we attempt to write a minimal model for the same. In this, there are three paramters in equation 2.1 that can be tuned, B, $L_0(t)$ and $F^\alpha(t)$. B is the elastic moduli of the spring junction and no experimental time dependant variance in this has been observed. $F^\alpha(t)$ is the active force that is also fixed by the cycle of Myosin pulses in the system. Hence we assume that the detailed balance violations are going to happen only by changes in $L_0(t)$. In every time step when $L_0(t)$ changes, the equilibrium rest length of the system changes too. As the L_0 value decreases, the system spring length will tend to a smaller and smaller value at every time step. There is now an obstacle for the system to go to previous larger values of L and hence it can work only in the unidirectional direction of shrinkage. A shrinking L_0 is acting as the 'pawl' for our ratchet.

Chapter 3

Minimal Model for rest length L_0

To write a minimal model for the rest length $L_0(t)$, We work under certain assumptions

1. The rest length shrinks for some timescale ΔT_1 which is the time when the E-Cadherin clusters are breaking apart. The velocity S_1 can be directly related to the rate of fragmentation of the trans E-Cadherin clusters.

2. Once the clusters have fragmented, the rest length can either remain static or increase in length for a time period of ΔT_2 when the monomers are aggregating to form trans clusters. The velocity S_2 can be directly related to the rate of aggregation of the trans E-Cadherin clusters which oppose shrinkage.

Under these assumptions, we build the minimal model of $L_0(t)$ as such:
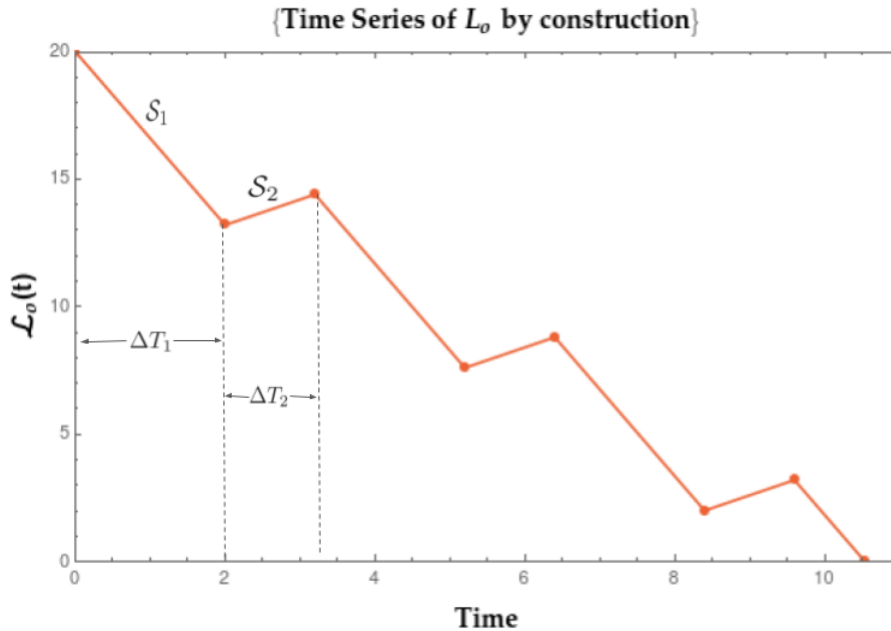
Figure 3.1: We construct the rest length $L_0(t)$ to shrink monotonically down to 0, controlled by 2 knobs S_1 and S_2 that dictate the rate of the decrease and increase. Each of the slopes is 'active' for the corresponding ΔT_1 or ΔT_2

For now, we can assume the shrinkage happens exactly when the myosin pulse is switched on ($\Delta T_1 = \Delta t_1$) and when the myosin pulse is switched of, the increase/no change takes place ($\Delta T_2 = \Delta t_2$). These assumptions can be relaxed later. This construction can be also be parametrised using 2 other relevant parameters.
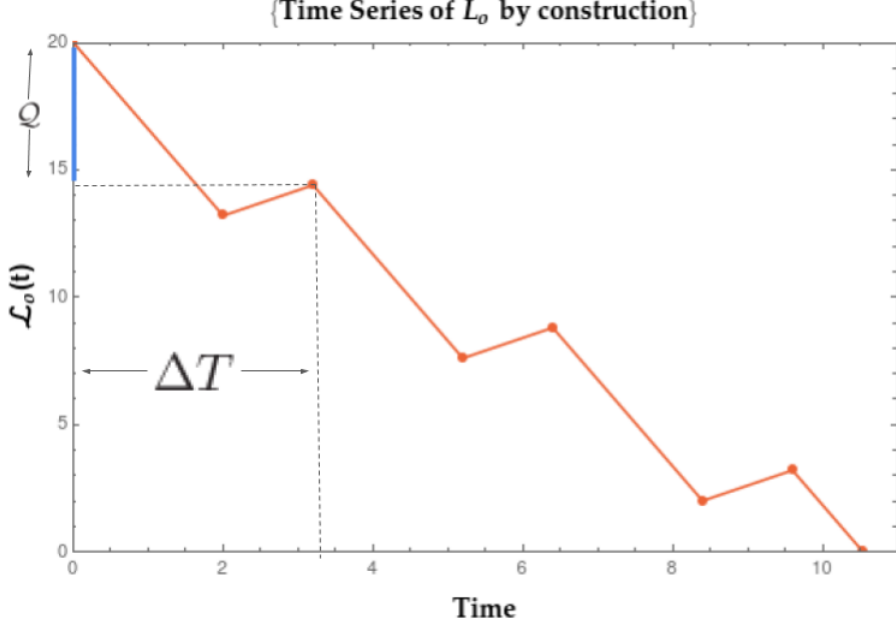
Figure 3.2: The monotonic decrease can also be parametrised by an offset $\mathcal{Q}$ and the total time ΔT over which a Myosin cycle takes place (one cycle is counted as the pulse being on and off, from the time it is switched on to when it is switched on again). The two knobs are now Q and ΔT

The parameter $\mathcal{Q}$ or the offset in L_0 over one entire turnover period ΔT is related to the E-Cad density after turnover. If the offset is 0, which means the rest length has come back to the same value after one cycle, E-Cad density is conserved. However if we have non-zero Q, E-Cad densities are not conserved and eventually, the rest length will shrink to zero. We define the ratio of $\frac{\Delta T_2}{\Delta T_1} := f$. Given f, we can use one parameter from 3.1 and 3.2 to get the full information or both the parameters from either of the set.

With the construction of L_0 and phenomenological choice of F^α, we should now be able to solve completely for $L(t)$. But we run into problems, the two biggest being

- The presence of two different timescales (can be 4 if the assumption is relaxed) in the problem which makes solving it in the continuum limit mathematically intractable.

- The presence of dimensional parameters.

To solve these problems, we discretise our equations and treat the L dynamics as a Markov process. This is reasonable as after every full-time period of ΔT, the process can be thought to have reset itself and begins, with different initial conditions. Hence it depends on the previous move merely for getting a position where it is to start from.

3.1   Solution of the equations

We discretise the equations first before we non-dimensionalise to fully capture the multiple time scales present.

For the purpose of consistency, we index each $L(t)$ by the index k after k moves have been made. Hence, L^k and L_0^k are the respective lengths after k moves have been made across both the time scales with L^{int} and L_0^{int} being the initial conditions at $t = 0$.

1. $k \in [0, 1, 2 \ldots)$

2. At $t = \Delta t_1$, our index is at $k = 1$ and hence L^1 and L_0^1.

3. At $t = \Delta t_1 + \Delta t_2$, our index is $k = 2$ and hence L^2 and L_0^2.

Now based on this new index, we can discretise based on whether k is odd or even, and accordingly the timescale will be Δt_1 or Δt_2 We first discretise our time with this index. Some calculations and phenomenology yields

$$t^k = \begin{cases} \frac{1}{2}k\Delta t_1 + \frac{1}{2}k\Delta t_2 & \text{; k is even} \\ \frac{1}{2}(k-1)\Delta t_2 + \frac{1}{2}(k+1)\Delta t_1 & \text{; k is odd} \end{cases}$$

which can be simplified to

$$t^k = \begin{cases} \frac{1}{2}k(1+f)\Delta t_1 & \text{; k is even} \\ \frac{1}{2}(k-1)f\Delta t_1 + \frac{1}{2}(k+1)\Delta t_1 & \text{; k is odd} \end{cases}$$

3.1.1   Constructing Difference Equations for L_0

We also construct L_0 from S_1 and S_2 for mathematical ease as all other information can be deduced from there. From the desired form of L_0 in the graph, we can write

$$L_0^{2k+1} = L_0^{2k} - S_1\Delta t_1 \tag{3.2}$$
$$L_0^{2k+2} = L_0^{2k+1} + S_2 f\Delta t_1 \tag{3.3}$$

The negative signs in the equation impose the constraint $S_1 > 0$ and $S_2 > 0$. Substituting one into the other, we get

$$L_0^{2k+2} = f S_2\Delta t_1 - S_1\Delta t_1 + L_0^{2k} \tag{3.4}$$

This is a second order recursive equation and hence should need two constants to solve.

These constants enter the solution as $C_1 + (C_2)^{2k}$ However, under the assumption of $k > 0$ and k is an integer, the constants can be removed by specifying the initial condition of $L_0^0 = L_0^{int}$ The solution of one recursion relation can again be substituted into the other one to give us the final solution as

$$L_0^{2k} = L_0^{int} + k(-S_1 + fS_2)\Delta t_1 \tag{3.5}$$

$$L_0^{1+2k} = L_0^{int} - S_1\Delta t_1 + k(-S_1 + fS_2)\Delta t_1 \tag{3.6}$$

3.1.2 Discretising the L dynamics

We discretise the differential equation using the first-order Euler's Method[3]. Depending on whether k is odd or even, we get:

$$\gamma\frac{L^{2k+1} - L^{2k}}{\Delta t_1} = -B(L^{2k} - L_0^{2k}) - \mathcal{A} \tag{3.7}$$

$$\gamma\frac{L^{2k+2} - L^{2k+1}}{\Delta t_2} = -B(L^{2k+1} - L_0^{2k+1}) \tag{3.8}$$

which are simplified to

$$\gamma(L^{2k+1} - L^{2k}) = B\Delta t_1(L^{2k} - L_0^{2k}) - \mathcal{A}\Delta t_1 \tag{3.9}$$

$$\gamma(L^{2k+2} - L^{2k+1}) = fB\Delta t_1(L^{2k} - L_o^{2k}) \tag{3.10}$$

3.1.3 Making the Equations Non-Dimensional

We define $\tilde{L} = \frac{L}{L^*}$ and $\tilde{\Delta t_1} = \frac{\Delta t_1}{t^*}$ where $(\cdot)^*$ is some characteristic quantity. In 3.9 and 3.10, we multiply by some characteristic length and characteristic time scale to get: Working on Eqn 3.9,

$$\gamma L^*(\tilde{L}^{2k+1} - \tilde{L}^{2k}) = -B\Delta t_1 L^*(\tilde{L}^{2k} - \tilde{L}_0^{2k}) - \mathcal{A}\Delta t_1 \tag{3.11}$$

To try and extract the characteristic length scale, we rearrange as

$$(\tilde{L}^{2k+1} - \tilde{L}^{2k}) = \frac{-B\Delta t_1}{\gamma}(\tilde{L}^{2k} - \tilde{L}_0^{2k}) - \frac{\mathcal{A}\Delta t_1}{\gamma L^*} \tag{3.12}$$

We extract a time scale from the system as:

$$(\tilde{L}^{2k+1} - \tilde{L}^{2k}) = \frac{-Bt^*\Delta t_1}{\gamma}(\tilde{L}^{2k} - \tilde{L}_0^{2k}) - \frac{\mathcal{A}\Delta t_1 t^*}{\gamma L^*} \tag{3.13}$$

This gives us the following values:

$$t^* = \frac{\gamma}{B} \tag{3.14}$$

$$L^* = \frac{At * \Delta t_1}{\gamma} \tag{3.15}$$

$$L^* = \frac{A\tilde{\Delta t_1}}{\gamma} = \lambda \tilde{\Delta t_1} \tag{3.16}$$

$$\lambda = A/B \tag{3.17}$$

We note that we have another quantity λ which is what we choose to rescale our lengths with it. We know,

$$\tilde{L} = \frac{L}{L^*} = \frac{L}{\lambda \bar{\Delta t_1}} = \frac{\bar{L}}{\bar{\Delta t_1}} \tag{3.18}$$

.

From the last equality, we get $(\bar{\cdot}) = (\cdot)/\lambda$ and we define $\tilde{\Delta t_1} = \bar{\Delta t_1} := \tau$

Finally, substituting these quantities into Eqn 3.9 and doing the same analysis for Eqn. 3.10, we get

$$\bar{L}^{2k+1} = \bar{L}^{2k} - \tau(\bar{L}^{2k} - \bar{L_o}^{2k} + 1) \tag{3.19}$$

$$\bar{L}^{2k+2} = \bar{L}^{2k+1} - f\tau(\bar{L}^{2k} - \bar{L_o}^{2k}) \tag{3.20}$$

We need to non-dimensionalise the dynamics of L_0 too. We use the definition from 3.18 to get the following

$$\bar{L_0}^{2k} = \bar{L_0}^{int} + k(-\bar{S_1} + f\bar{S_2})\tau \tag{3.21}$$

$$\bar{L_0}^{2k+1} = \bar{L_0}^{int} - \bar{S_1}\tau + k(-\bar{S_1} + f\bar{S_2})\tau \tag{3.22}$$

$$S_i^* = \frac{\lambda}{t^* S_i} \tag{3.23}$$

This gives us the dynamic equations to describe our system (Where we drop the bar for ease of notation).

Dynamic Equations for the system

$$L^{2k+1} = L^{2k} - \tau(L^{2k} - L_0^{2k} + 1)$$

$$L^{2k+2} = L^{2k+1} - f\tau(L^{2k} - L_0^{2k})$$

$$L_0^{2k} = L_0{}^{int} + k(-S_1 + fS_2)\tau$$

$$L_0^{2k+1} = L_0{}^{int} - S_1\tau + k(-S_1 + fS_2)\tau$$

3.2 Initial Conditions

Since we have two length scales(L and L_0) to begin with, it becomes important to decide what the difference between them should be, if at all. As it turns out, for this system, the only condition that makes logical sense is the initial conditions of $L_0^{int} = L_{int}$. Experimentally, we know that the cell junction exists without fluctuations before the junction shrinkage is initiated. The only situation in which this will happen is if the initial condition, prior to initiation of shrinkage, is the equilibrium position. The junction length L must be equal to the rest length L_0 at the beginning and then change following the dynamic equations.

3.3 Analysis of the Minimal Model for L_0

We want to ask what are the conditions under which our system is a ratchet. We also want to explore any features or subtleties that we may find and eventually, make thermodynamic arguments for the same.

3.3.1 When is our system a ratchet?

Since any spring tries to minimise its energy by relaxing to the rest length L_0, if we want the spring length to ratchet to 0, the rest length must do so too. To calculate conditions for this, one can by eye get condition given in boxes 1. Alternatively, it can be derived as follows:

1. Let K_{max} be the number of moves the by the L_0 protocol such that $L_0^{K_{max}} = 0$

2. This can be at the even move or the odd move. Hence we solve for 2 equations 3.21 and 3.22 both.

3. We take the minimum value as we stop at the first moment when the rest length is zero. Beyond this K_{max}, the rest length will become negative which will change the fundamental dynamics of the spring in an unphysical manner and hence we can discard this regime.

4. We solve for the minimum of $L_0{}^{2k} = L_0{}^{int} + k(-S_1 + fS_2)\tau = 0$ and $L_0{}^{2k+1} = L_0{}^{int} - S_1\tau + k(-S_1 + fS_2)\tau = 0$ to give us

$$K_{max} = Min(\frac{L_0^{int}}{S_1 - S_2 f}\tau, \frac{L_0^{int} - S_1\tau}{S_1 - S_2 f})$$

Note: We have dropped the bar for convenience of notation. All quantities are dimensionless. For this K_{max} to be positive (negative number of moves are not defined), we get 2 conditions.

1. **Condition 1:** $S_1 > S_2 f$
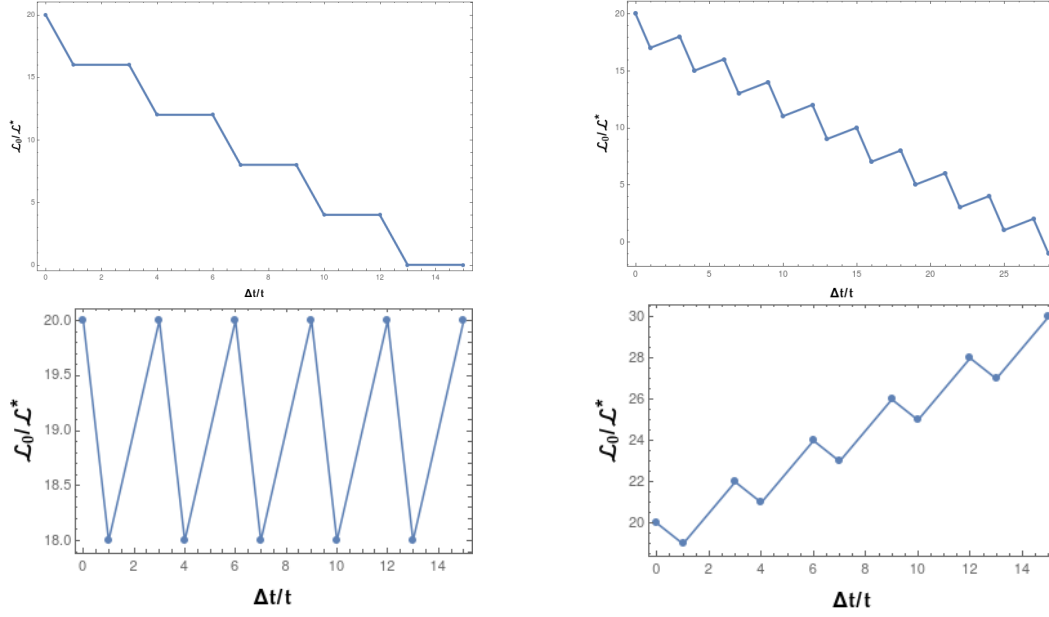
Figure 3.3: Testing L_0 Dynamics for various parameters in Condition 1.
Top Left: $S_1 > S_2 f$ at $S_2 = 0$. L_0 shrinks to 0 in a finite number of steps and hence is allowed. **Top Right:** $S_1 > S_2 f > 0$. L_0 shrinks to 0 in a finite number of steps and hence is allowed. **Bottom Left:** $S_1 = S_2 f$. At equality, L_0 does not shrink to 0, instead it oscillated between 2 values. Strict inequality must be obeyed to get a physically relevant rest length. **Bottom Right:** $S_1 < S_2 f$ Rest length will never shrink to 0 and continue to grow positively.

> This gives us an upper bound on aggregation of trans E-Cadherin clusters. If aggregation happens faster than this rate (dependant on fragmentation rate), the ratchet does not shrink to zero.

2. **Condition 2:** $S_1 < \frac{L_0^{int}}{\tau}$
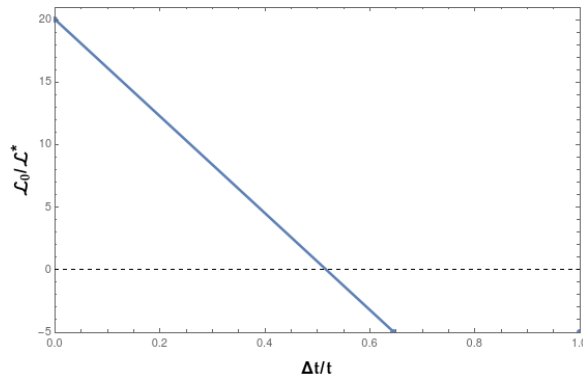
Figure 3.4: Here, we get an upper Bound on S_1. When this condition is violated, the rest length shrinks to 0 in the very first step which is un-physical

> If the rate of fragmentation is very high, the length will immediately shrink to zero. The tissue may buckle or tear in this regime.

16

3.4 Dynamics of L

Working within the conditions from the previous section, we want to see how our minimal model affects the observable dynamics of the junctional length L. We fix value of $f = 3/5$ from experiment[13] and vary S_1, S_2 to get various dynamics. We can get multiple kinds of paths by tuning the knobs of S_1 and S_2.
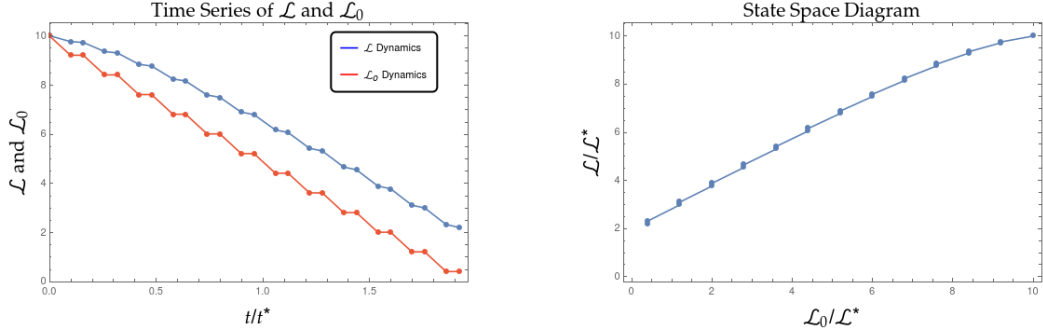
Figure 3.5: Chosen values of $S_1 = 4$ and $S_2 = 0$. We see the junction length L in blue and rest length L_0 in red (on the vertical axis in a.u) shrinks to 0 monotonically as time goes on (on the horizontal axis, non-dimensionalised by characteristic time t^*). Backlash error is minimised and this can be categorised as a 'Good Ratchet'. On the right, the state space diagram of this path.
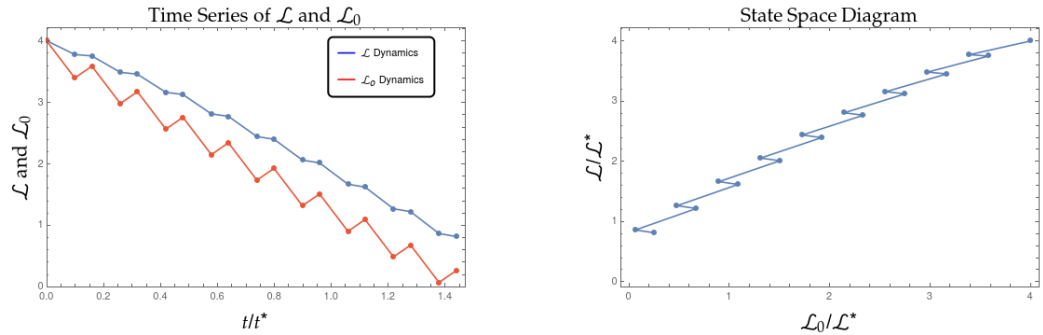
Figure 3.6: Chosen values of $S_1 = 4$ and $S_2 = 0$. We see the junction length L in blue and rest length L_0 in red (on the vertical axis in a.u) shrinks to 0 as time goes on (on the horizontal axis, non-dimensionalised by characteristic time t^*). As we increased the S_2 value from zero to a finite number, or the rate of aggregation of trans-clusters, the ratchet still exists but there is some backlash error. This makes sense because as we increase the aggregation of trans-clusters, we expect opposition to the shrinkage to grow too. On the right, the state space diagram of this path. The backlash can be seen more clearly in the state diagram.
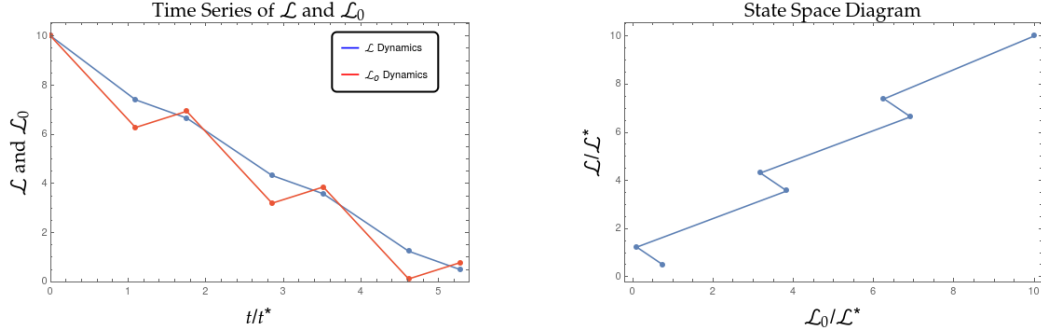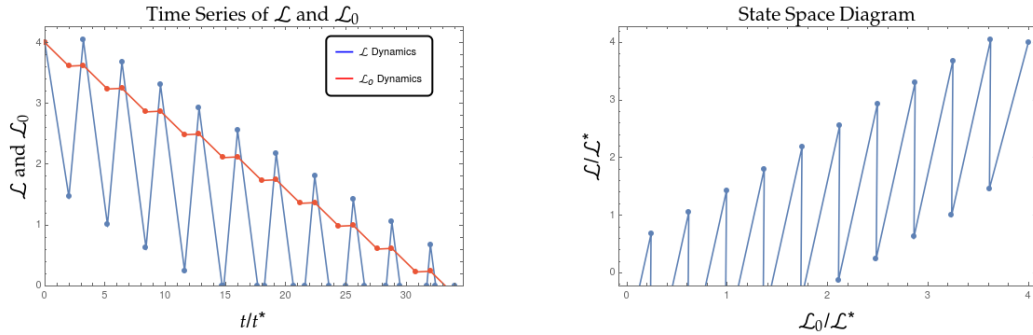
Figure 3.7: Chosen values of $S_1 = 2$ and $S_2 = 1$. We see the junction length L in blue and rest length L_0 in red (on the vertical axis in a.u) shrinks to 0 as time goes on (on the horizontal axis, non-dimensionalised by characteristic time t^*). As we reduced the S_2 value or the rate of aggregation, as well as the S_1 value or the rate of fragmentation, we observe two things: the number of steps to shrink to zero falls and the backlash error increases. On the right, the state space diagram of this path. The backlash can be seen more clearly in the state diagram.

Figure 3.8: Chosen values of $S_1 = 0.01$ and $S_2 = 3$. As we decrease the rate of fragmentation to smaller and smaller value, we can expect more opposition to shrinkage as trans-clusters are not breaking apart. We see the junction length L in blue and rest length L_0 in red (on the vertical axis in a.u) does shrink to 0 as time goes on (on the horizontal axis, non-dimensionalised by characteristic time t^*). However, there is a high amount of backlash error and this can be classified as a 'Bad Ratchet'. On the right, the state space diagram of this path. The backlash can be seen more clearly in the state diagram.

We observe that both the fragmentation and aggregation rates of the trans-clusters of E-Cad seem to affect the junctional length dynamics. There is also a different quantity that can be used as a parameter. From Fig. 3.2, we know $\mathcal{Q}$ is the offset in junctional length L in a cycle. This can be thought of as a more relevant parameter as it can directly be connected to E-Cadherin densities, independent of the densities of trans and cis clusters. A zero offset would imply no 'leakage' of E-Cadherin density in a given cycle and we shall see consequences of this in section 3.6. We can write

$$\mathcal{Q} = (S_1 - S_2 f)\tau \tag{3.24}$$

which allows us to still vary the 2 knobs of S_1 and S_2. The condition from 3.3 holds here as the offset must be greater than 0.

3.5 Phase Diagrams in the System

One measure to quantify the 'goodness of a ratchet' is the amount of "backlash" that the ratchet undergoes. We can either quantify the entire accumulated backlash error over the entire process or the average backlash error in 1 cycle ΔT. We try to find phase diagrams in the S_1, q space. We want to tune the offset $\mathcal{Q}$ and the fragmentation rate s_1 as our knobs. To ensure consistency, we perform the following calculation:

1. From 3.24, we get

$$S_2 = S_2(S_1, \mathcal{Q}) = \frac{S_1 - \frac{\mathcal{Q}}{\tau}}{f} \tag{3.25}$$

2. This gives us a lower bound on S_1 to ensure that $S_2 > 0$ as $S_1^{min} = \frac{\mathcal{Q}}{\tau}$

3. Now we can tune $\mathcal{Q}$ and S_1 which will automatically tune S_2 to fit into our current paradigm.

4. To ensure that each S_1 and $\mathcal{Q}$ are sampled equally and without bias, we define $N =$ number of points in the phase diagram. We also define $\delta S = \frac{S_1^{max} - S_1^{min}}{N}$ where s_S^{min} and S_1^{max} come from 3.25 and 3.3

We also fix $\tau = 0.5, f = 3/5$ for the following set of graphs.

3.5.1 Phase Diagram in total accumulated error for the ratchet
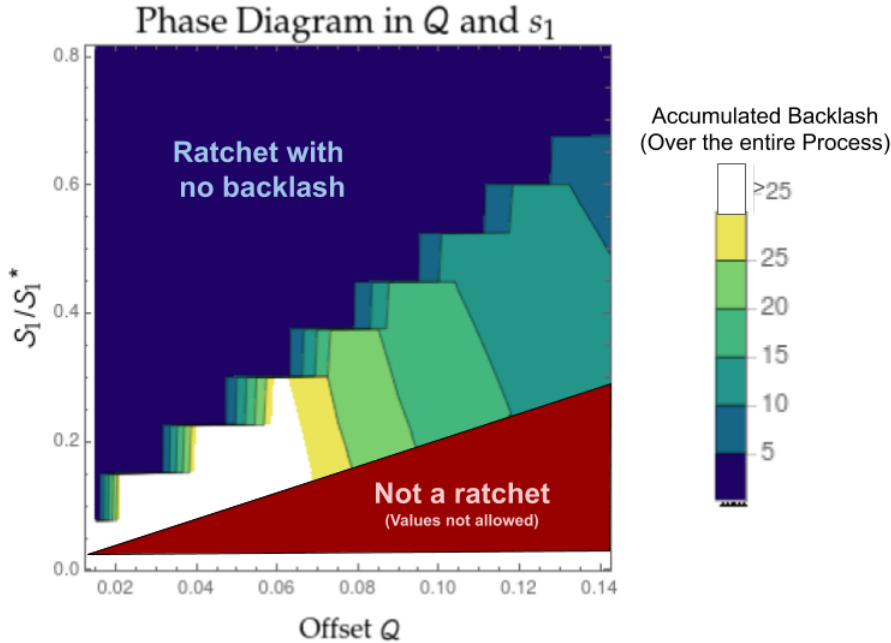
Figure 3.9: By tuning the 2 parameters using the protocol above,we obtain this phase diagram. The horizontal axis has the offset $\mathcal{Q}$ and the vertical axis has the non-dimensionalised rate of fragmentation of trans-clusters S_1. On the diagram itself, the total accumulated backlash error is plotted in color as a heat map (with the legend showing values). Extremely high values of backlash error has been marked in white to allow us to visualise other features in the diagram.

We can see three regimes in the phase diagram. The first regime, marked in red, has values of S_1 and $\mathcal{Q}$ that are not allowed within the physical limits. The system is not a ratchet in this case. The second regime, marked in Royal Blue, is the regime where all values give us a monotonic decrease in junction length L and we see no backlash error. The third regime, marked in color (and white) exists as a ratchet but we see varying amounts of backlash error. Some of these are good ratchets, some bad. The white area denoting extremely high values of error also exists for $\mathbf{Q} = 0$. We can see the features of the white area by zooming in to that.
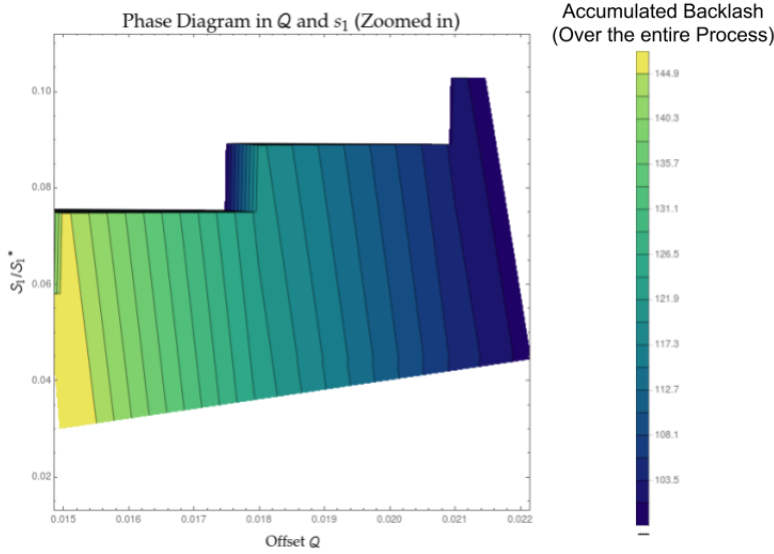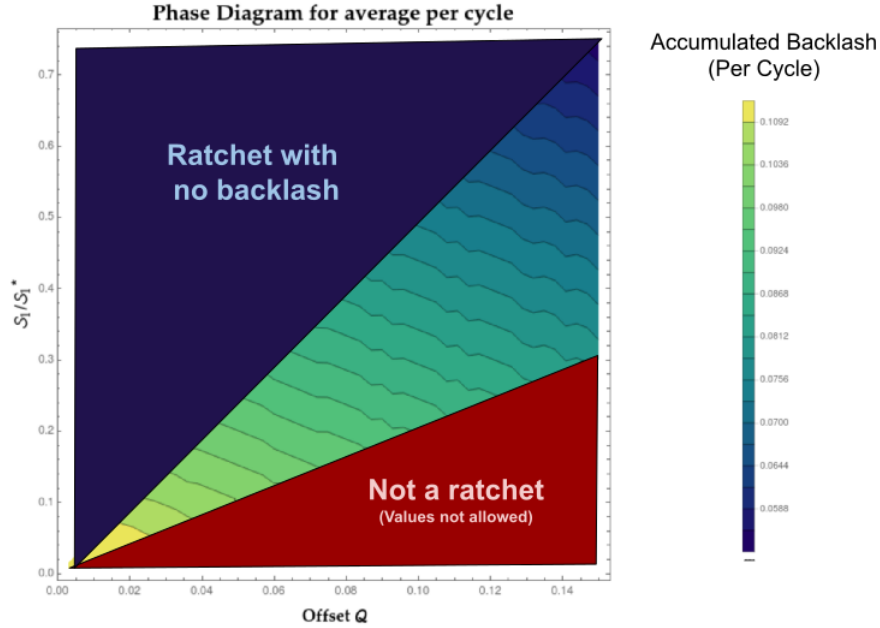

Figure 3.10: By tuning the 2 parameters using the protocol above,we obtain this phase diagram. The horizontal axis has the offset $\mathcal{Q}$ and the vertical axis has the non-dimensionalised rate of fragmentation of trans-clusters S_1. On the diagram itself, the total accumulated backlash error with values above 25 a.u. is plotted in color as a heat map (with the legend showing values). The same vertical contours, following the same trend are seen, with just a higher value or error.

From the phase diagrams, we observe that the error in the ratchet is very sensitive to changed in the offset $\mathcal{Q}$. For a fixed value of $\mathcal{Q}$, changing the value of S_1 keeps us in the same countour with minimal change in error. However, by fixing S_1 and changing Q, we pass through multiple contours.

3.5.2 Phase Diagram in the accumulated error averaged over the each Myosin Pulse Cycle

An argument can be made that the quantity plotted above is not the best quantity. The error for smaller values of S_1 and $\mathcal{Q}$ can be much higher as each step size is smaller and hence the ratchet will take many more steps to shrink to zero(resulting in the accumulated error being much larger). To correct for this, we average over the number of Myosin cycles to get the average error per cycle. We plot the same phase diagram of backlash error averaged over the number of cycles.

Figure 3.11: By tuning the 2 parameters using the protocol above,we obtain this phase diagram. The horizontal axis has the offset $\mathcal{Q}$ and the vertical axis has the non-dimensionalised rate of fragmentation of trans-clusters S_1. On the diagram itself, the total accumulated backlash error, averaged over the number of Myosin Pulses, is plotted in color as a heat map (with the legend showing values). We see three regimes again

We immediately notice that the features at the boundary get smoothed out over the average. This indicates that these were small errors merely accumulated over a large number of steps.

However, this parameter can also be deceptive. Overall, the cell may not care whether the average error is low if the total error accumulated over the whole process may be larger than cell junction can tolerate. More in depth understanding may be needed to choose a better parameter.

Noticeably, we observe that at offset equals zero, there seems to be a very large value of backlash error, no matter what the value of S_1 is. We explore this case of zero offset in a little more detail.

3.6 Zero Offset Case: E-Cadherin levels are conserved

When the offset $\mathcal{Q}$ is zero, it corresponds to fixed E-Cadherin levels. Essentially, after each cycle of the myosin pulse switching on and off, the E-Cadherin levels reset back to their prior values. This will directly affect that rest length $L_0(t)$ dynamics as there will be no offset in the rest length either.
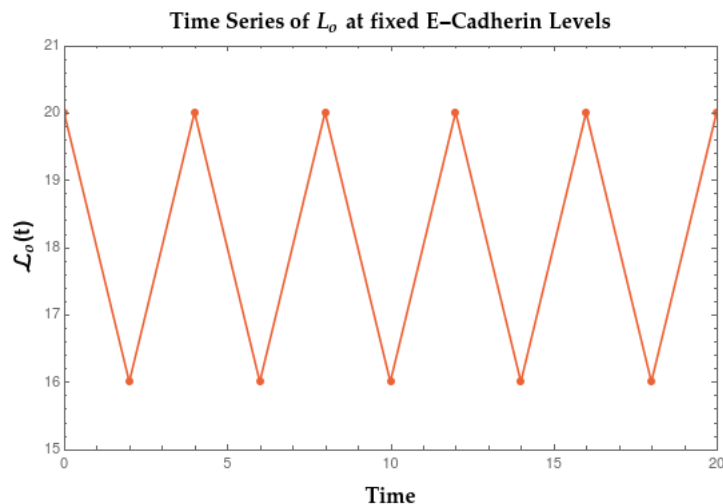
Figure 3.12: The dynamics of rest length L_0 with fixed E-Cad levels. The horizontal axis has time and the vertical axis has the rest length in a.u. Since the offset is zero, the rest length always oscillates between two values (The initial value and the value it drops to initially). This happens infinitely and it does not shrink to 0 in a finite number of steps.

We see if E-Cadherin levels are fixed, the rest length will never shrink to zero. Hence, the L dynamics will also never shrink to zero and our system will not a ratchet at all. This can also be observed by plotting all error values observed in the phase diagram.
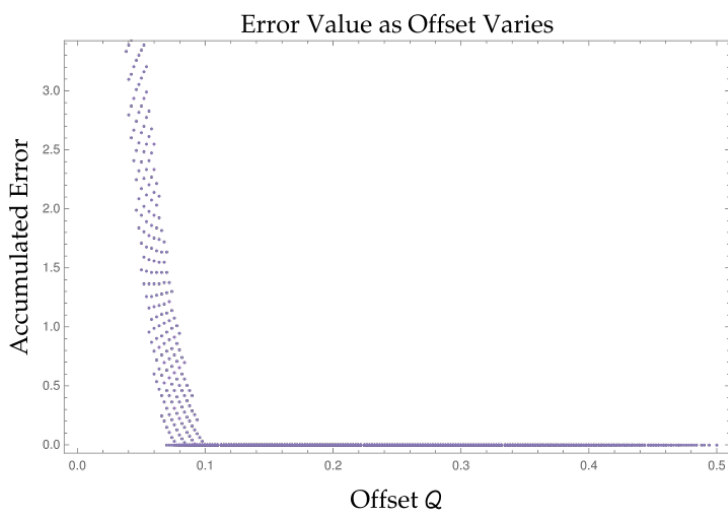
(a) Plotting the error (on the vertical axis in a.u) with varying offset Q (on the horizontal axis). As we approach $Q = 0$, the error tends to asymptotically approach ∞. At $Q = 0$, the system will never ratchet to zero and oscillate between two values.

As we asymptotically approach $\mathcal{Q}$, the error asymptotically approaches ∞. This supports the fact that the junctional length never goes to zero as this value of accumulated backlash is possible only if the length keeps 'zig-zagging' (the L_0 dynamics do the same). **This implies that we cannot have a reliable ratchet at $\mathcal{Q} = 0$ or fixed E-Cadherin levels. There must be some 'leakage' of E-Cadherin, some turnover for a reliable ratchet to exist. The density of E-Cadherin must decrease after each subsequent pulse. This is seen as there is always a ratchet, for large enough S_1 values for every non-zero offset.**

There must be E-Cadherin turnover with non-conserved E-Cadherin density for a reliable ratchet

---

3.7   Leanings from the minimal model

The preceding model gives us important observations with regards to the offset in E-Cadherin levels Q. This toy model, while making some useful predictions, suffers from some major flaws too.

1. There is no experimental access to the rest length L_0 of the system. Since the model hinges on construction of the L_0 dynamics, we can tune it in the model to get various dynamics but not have any tests for veracity of our model.

2. Our tunable parameter is also something that is not tunable in the actual system, The equilibrium rest length is a hypothetical property of the cell junction that we cannot control.

3. This toy model was constructed to gain a basic intuition. As such, there is no strong rational for a linear decay within a time interval.

4. In the model that we have constructed, the decrease in L_0 which corresponds to the decrease in E-Cadherin levels is same across all time intervals. One can argue this would not be the case. In each time interval($\Delta T_1 + \Delta T_2$ from Figure 2.8), when the Myosin pulse kicks in, it is akin to a reset. The E-Cadherin leakage starts from a lower level of E-Cad density from the previous cycle. We can reasonably assume that there should be some time dependence to the offset.

However, this flawed model also makes some useful predictions. We can see that the relevant quantity to consider is infact the reduction in E-Cadherin density or the leakage. We have already proved that this must exist in the system to get a ratchet from section 3.6. Even from the phase diagrams in section 3.5 , we can see that the backlash error is sensitive to changed in Q more than the rate of fragmentation or aggregation. This is also a parameter that can also be experimentally observed (indirectly). Hence, we take this offset to be a relevant parameter, with some assumptions and caveats.

Chapter 4

New Model with Time Varying Offset

We now want to better our model by choosing a time dependant, decaying function of $Q(t)$. We also want to choose this $Q(t)$ as a quantity that acts after one Myosin pulse in a time period τ_m to avoid microscoping details at smaller time scales that we cannot observe. We can choose different forms for $Q(t)$ under the following assumptions.

1. The $Q(t)$ must never go down to zero as a non-zero offset is required for ratcheting (Section 3.6)

2. $Q(t)$ must not take negative values in the regime we are looking at. We don't necessarily need a strictly positive function over all it's domain, merely till the ratchet is achieved, if at all.

3. The function must be monotonically decreasing. This assumption stems from the fact that at each time cycle of the L dynamics, the myosin pulse "resets" the system. Hence the leakage starts from a lower E-Cadherin density value that before.

4.1   Setting up the system

Since we have no access to the inner dynamics of the rest length L_0, we don't construct it explicitly. From Figure 3.2, we can see that after each cycle of the myosin pulse, the rest length falls by our defined value Q. In terms of discrete dynamics, we can define our new rest length dynamics as:

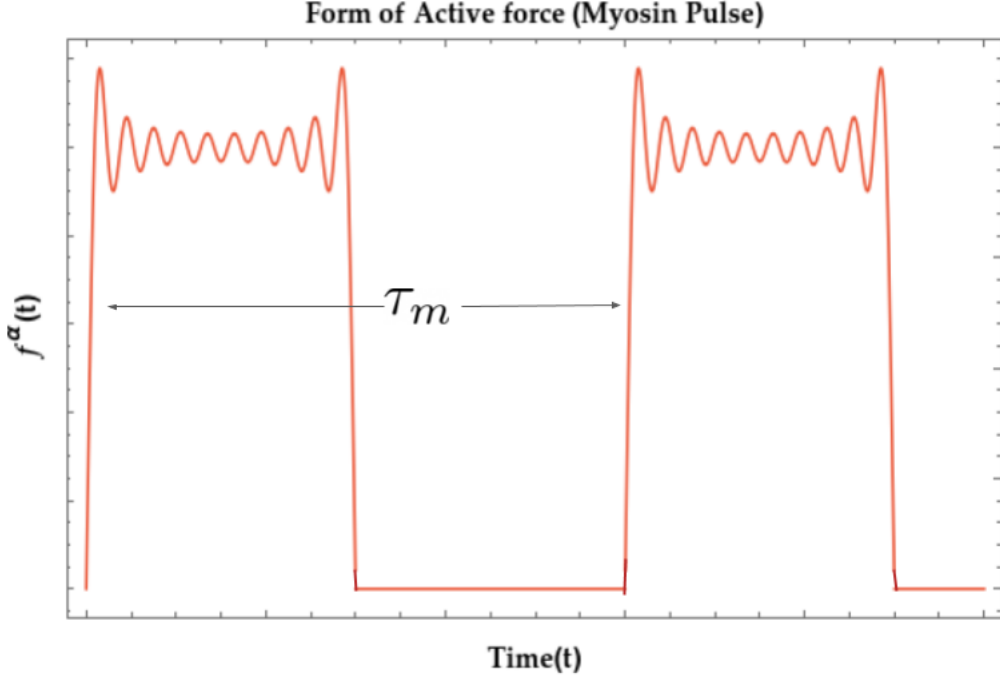$$L_0^k = L_0^{int} - \sum_{i=1}^{k} Q^k \tag{4.1}$$

This discretisation will change for every form of Q we choose.

Since we do not know the internal dynamics of the rest length in given time interval, we redefine the form of the active force over a time period τ_m such that it takes the given form.

$$F^\alpha(t) = \mathcal{A}f_\alpha(t) \tag{4.2}$$

where

$$f_\alpha(t) = \sum_{n=1,3,5..}^{20} \frac{1}{n}\sin(\frac{n\pi t}{\tau_m}) \tag{4.3}$$

Figure 4.1: We redefine our active force F^α in our new paradigm. The time is marked on the horizontal axis and the amplitude is marked on the vertical axis (in a.u.). It has only one time scale as we care only about the offset Q over one time period τ_m. We have also chosen a continuous form for it now.

This enters the spring equation normally as $L_0(t)$. Since we know longer have the "odd" and "even" move of the previous toy model, we do not need two separate equations. Using the same discretisation and non-dimensionalisation protocol as in Section 3.1.3, we get the following equation:

$$L^k = L^{k-1} - \tau(L^{k-1} - L_0^{k-1} + f_\alpha^{k-1}) \tag{4.4}$$

This is recursively solved to give us the following equation:

$$L^k = (1-\tau)^{k-1}(L^{int}(1-\tau) + \sum_{j=0}^{k-1}\frac{\tau}{(1-\tau)^k}(f^j - L_0^j)) \tag{4.5}$$

We can see that $\tau = 1$ leads to a singularity and instability in the system and must be worked around. We now explore the dynamics for different functional forms of Q.

25

4.2 Exponential Decay in Q

For the first functional form, we choose

$$\mathcal{Q}(t) = q_0 e^{\frac{q_s}{t}} \tag{4.6}$$

This reaches a minimum value of q_0 at large values of t, ensuring that the offset is always monotonically decreasing. The rate of decay is controlled by the parameter q_s. Using this form of the offset in Equation 4.1, we get the following form for L_0
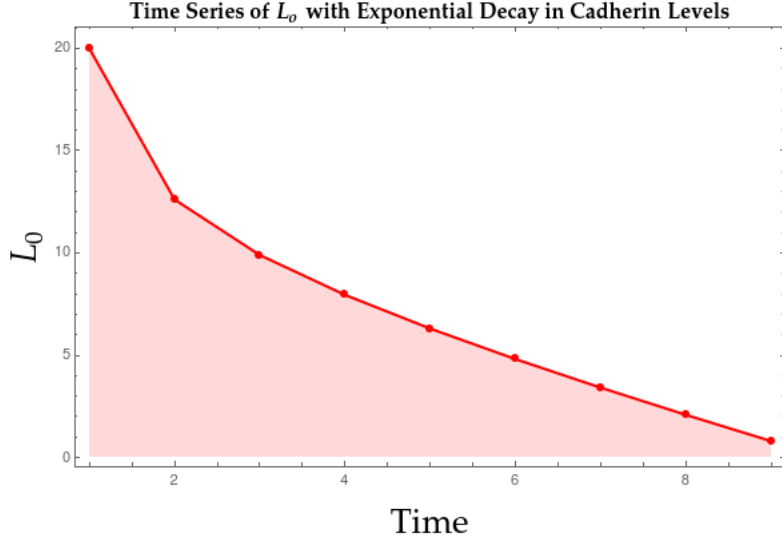

Figure 4.2: The time evolution (on the horizontal axis) of rest length with exponential decay (on the vertical axis in a.u.). This asymptotically approaches the value of q_0. For the above figure, $q_0 = 1$ and $q_s = 2$ for illustrative purposes.

A careful interplay between the minimum value q_0 and the rate of decay q_s is needed to ensure that the rest length does not crash to zero in a single step. Only values in which the rest length reduces to less than or equal to zero in less than one step are disallowed. Upper bounds for reasonable dynamics do exist but cannot be calculated for one parameter independent of the other.

Using this form of L_0, we plot the dynamics of the junction length in Figures 4.3-4.6 and 4.7-4.8. Straight away, we notice that as we increase q_s or the rate of decrease of the offset in Cadherin density Q, the shrinkage happens more rapidly. With increasing q_s, we also see the graph change shape qualitatively, from a straighter line to a more convex shape. This change is mirrors even as we decrease the minimum value q_0 that the offset Q can take. This can be seen by comparing Figures 4.3 and 4.5 with higher $q_s = 0.1$ and changing q_0 as well as Figures 4.4 and 4.5 with lower $q_s = 2.1$ and changing q_0. This makes sense as changing q_s changes the behaviour of rest length dynamics. However, it appears that as we reduce the minimum value q_0, the quality of the ratchet decreases and backlash errors start to accumulate.
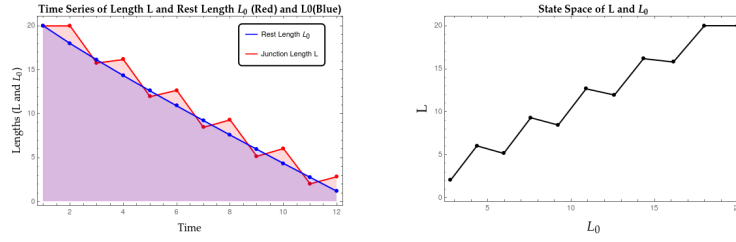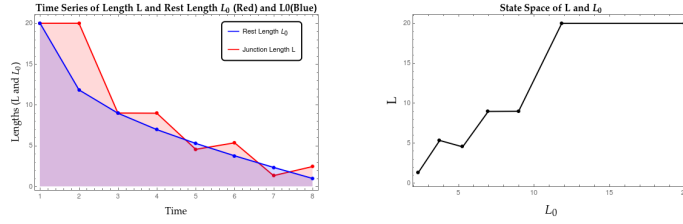
Figure 4.3: The horizontal axis shows time and the vertical axis shows length (in a.u.). The rest length L_0 is marked in blue and the junction length L is marked in red. For $q_0 = 2.0$ and $q_s = 0.1$, we see a ratchet exists with some backlash error. ($\tau = 1.1$)
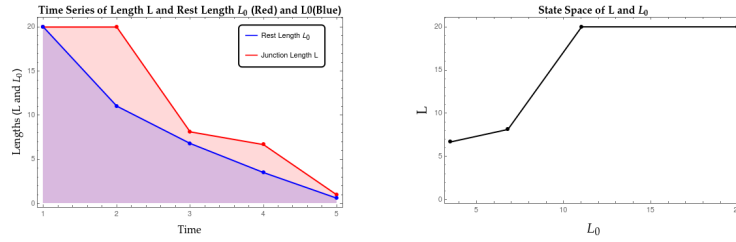
Figure 4.4: The horizontal axis shows time and the vertical axis shows length (in a.u.). The rest length L_0 is marked in blue and the junction length L is marked in red. For $q_0 = 2.0$ and $q_s = 2.1$, we see a ratchet exists with some backlash error. As we increase the rate of decay q_s, we see the number of steps in the process fall sharply. ($\tau = 1.1$)
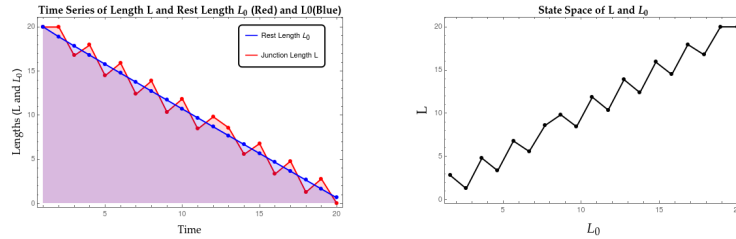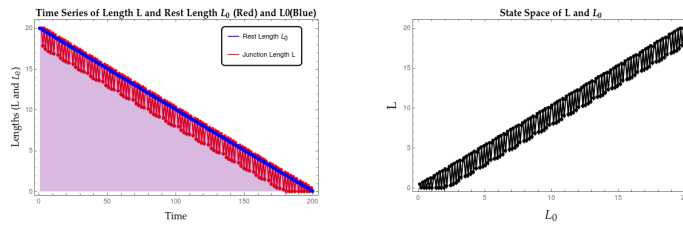

Figure 4.5: The horizontal axis shows time and the vertical axis shows length (in a.u.). The rest length L_0 is marked in blue and the junction length L is marked in red. For $q_0 = 1.0$ and $q_s = 0.1$, we see a ratchet exists with some backlash error. As we increase the rate of decay q_s and the minimum value of the offset q_0, the backlash errors seem to start accumulating faster that a higher minimum offset value. ($\tau = 1.1$)
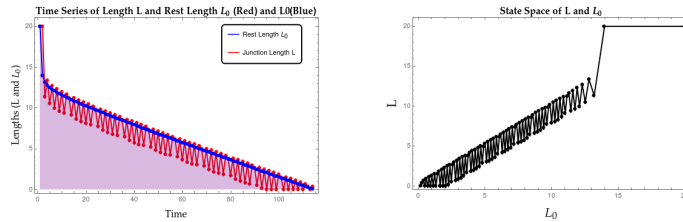
Figure 4.6: The horizontal axis shows time and the vertical axis shows length (in a.u.). The rest length L_0 is marked in blue and the junction length L is marked in red. For $q_0 = 1.0$ and $q_s = 2.1$, we see a ratchet exists with backlash error. As we increase the rate of decay q_s for the same minimum value of the offset q_0, the number of steps in the process fall sharply. ($\tau = 1.1$)

Figure 4.7: The horizontal axis shows time and the vertical axis shows length (in a.u.). The rest length L_0 is marked in blue and the junction length L is marked in red. If we choose $q_0 = 0.1$ (very low) and $q_s = 0.1$, we see a sharp increase in the number of steps. A bad ratchet exists with a large amount of backlash error. ($\tau = 1.1$)
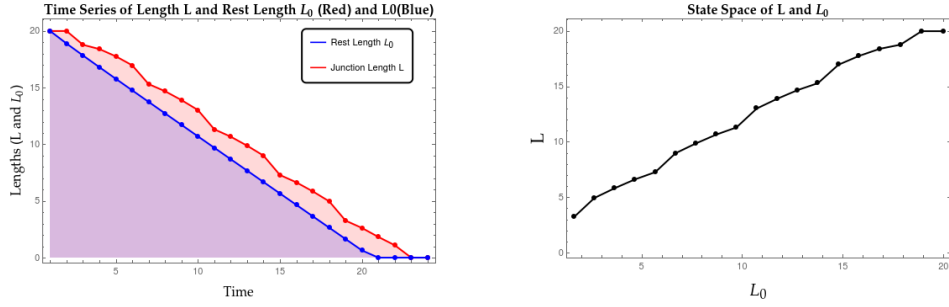

Figure 4.8: The horizontal axis shows time and the vertical axis shows length (in a.u.). The rest length L_0 is marked in blue and the junction length L is marked in red. If we choose $q_0 = 0.1$ (very low) and increase $q_s = 2.1$, the number of steps in the process do fall. We still observe a bad ratchet with a large amount of backlash error. ($\tau = 1.1$)

The previous paths were calculated at $\tau = 1.1$ which is a value greater than the singularity at $\tau = 1$. We repeat the same analysis for a value of $\tau = 0.4$ in Figure 4.9-4.10 at lesser than the singularity and qualitatively see the same shapes of the curves, but with much smaller number of steps implying faster shrinkage. We also notice that the rest length shrinks to zero faster than the junction length does in this case.
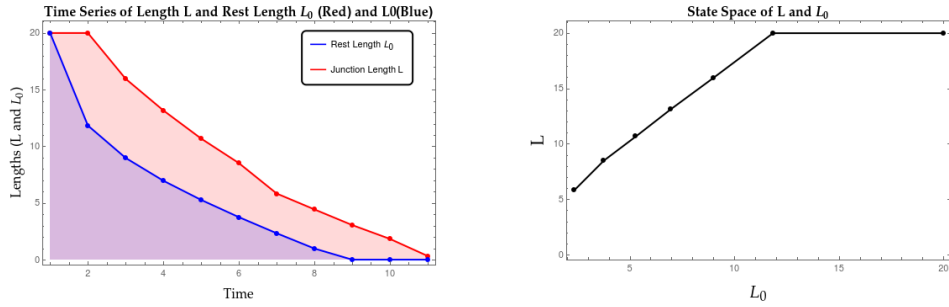

Figure 4.9: The horizontal axis shows time and the vertical axis shows length (in a.u.). The rest length L_0 is marked in blue and the junction length L is marked in red. For $q_0 = 1.0$ and $q_s = 0.1$, we see a good ratchet exists with very less backlash error. ($\tau = 0.4$)


Figure 4.10: The horizontal axis shows time and the vertical axis shows length (in a.u.). The rest length L_0 is marked in blue and the junction length L is marked in red. For $q_0 = 1.0$ and $q_s = 2.1$, we see a ratchet exists with minimal backlash error. The shape of the curve seems slightly different due to the first initial drop ($\tau = 0.4$)

4.2.1 Phase Diagram of Accumulated Error for exponential decay in E-Cad offset Q

To get a more comprehensive picture of which regime gives us a better ratchet, we plot the phase diagram in total accumulated backlash error.
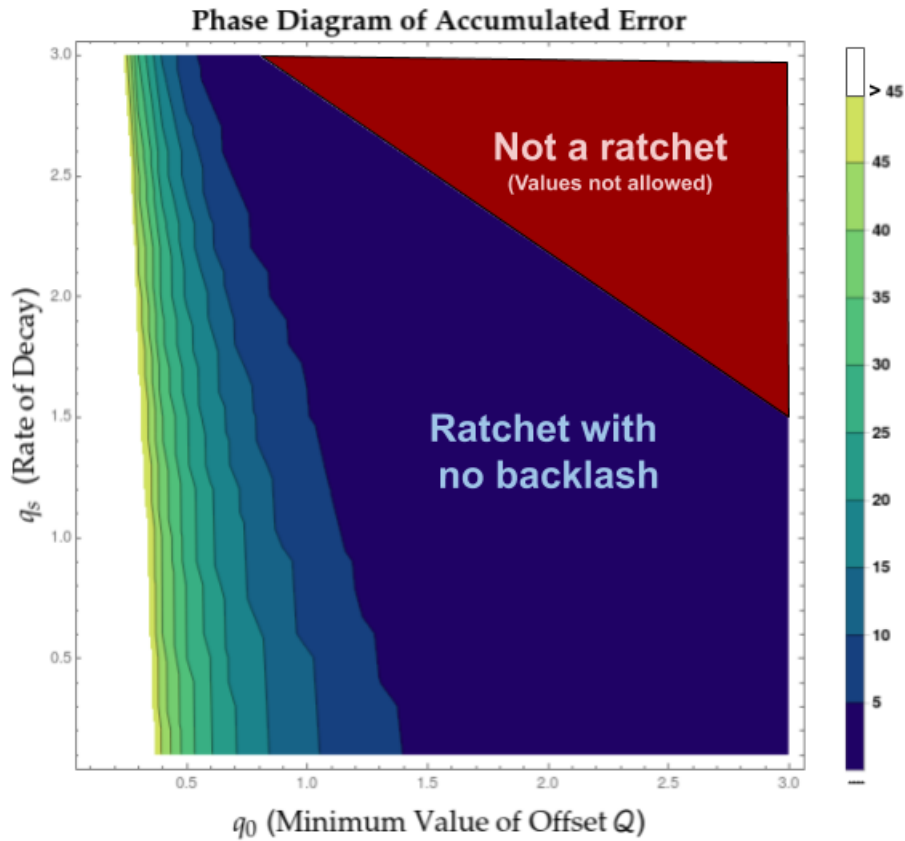
Figure 4.11: Phase Diagram for Accumulated Error in Q with exponential decay. We see three regimes. The horizontal axis has the minimum value of offset Q and the vertical axis has the rate of decay q_s. On the diagram itself, the total accumulated backlash error in color as a heat map (with the legend showing values). The regime marked in red is where the rest length crashes to zero in the very first step and hence is disallowed, marked as not a ratchet. We also observe a dark blue area of a good ratchet with no backlash errors. As we go to smaller rates of decays and minimum offset values, we see the amount of backlash error quickly tends to become very large.

We can observe that there is an optimum rate of decay for the offset. If this is too slow or decays to a very low value, we get large backlash errors. If this decay is very fast, the system does not exist as a ratchet at all.

4.3 Power Law decay in Q

We can also have a power law decay in the offset in Cadherin density.

$$\mathcal{Q}(t) = q_0 t^{-q_s} \tag{4.7}$$

The form for Q will decrease for all positive values of q_s. The exponent has been called q_s only for consistency. At very large values of t or q_s, the function does tend to 0, corresponding to know change in the offset of Cadherin density but in a time discrete system, we do not expect to reach such large values. Again, all parameters within a reasonable domain can be explored with no disallowed values mathematically. The reasonable domain excludes any values in which the rest length crashes to negative values in the first move. The exponent can be tuned to get varying dynamics for rest length L_0 as given below.

(a) $q_0 = 1.0$ and $q_s = 0.1$ **(b)** $q_0 = 1.0$ and $q_s = 1.5$
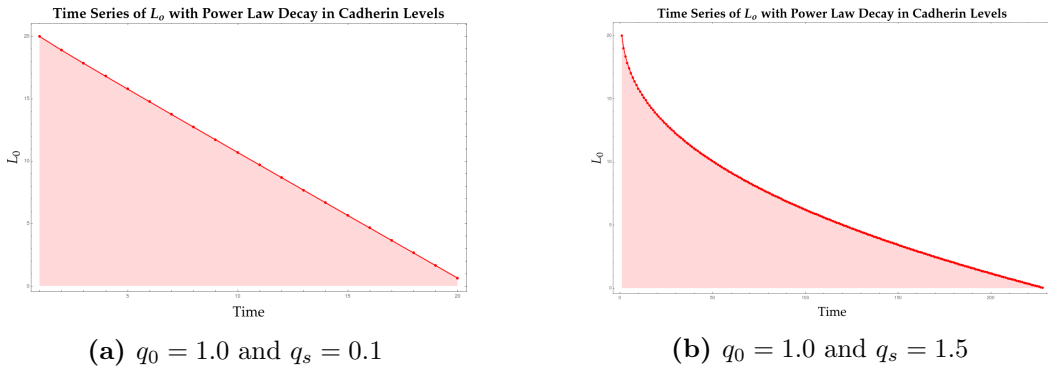
Figure 4.12: Different Behaviors exhibited by L_0 with power law decays in Cadherin density levels can be observed as time evolves (horizontal axis). The rest length (marked on the vertical axis in a.u) exhibits different behaviours and curves as we tune the exponents. A steeper exponent as in **b** shows a flatter curve.

The q_0 controls the amplitude of the decay and does not effect qualitatively the behavior of the rest length dynamics. It increases or decreases the number of steps in the shrinkage and the reasonable domain is controlled largely by the exponent.

While plotting, we see that we cannot push the q_s value much above 1 as that quickly pushes the change to zero and we do not obtain ratcheting. This reaffirms the fact that the ratcheting cannot be too steep or fast. Naturally, as we increase the minimum value q_0, we can explore higher exponentials and steeper shrinkage. This is illustrated in Figure 4.13, calculated at $\tau = 1.1$.
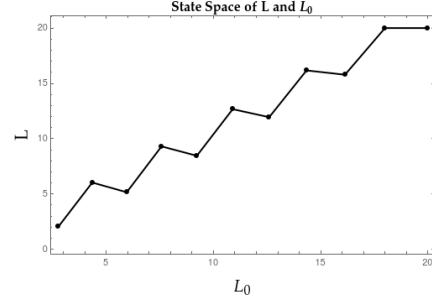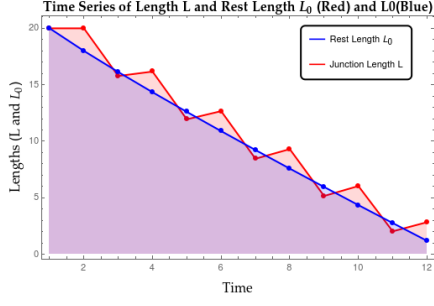
(a) $q_0 = 2.0$ and $q_s = 0.1$
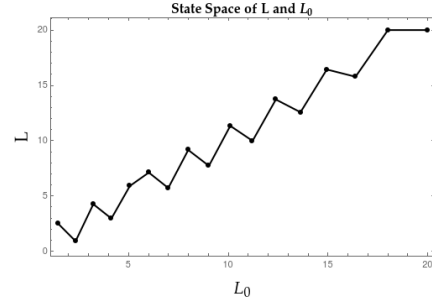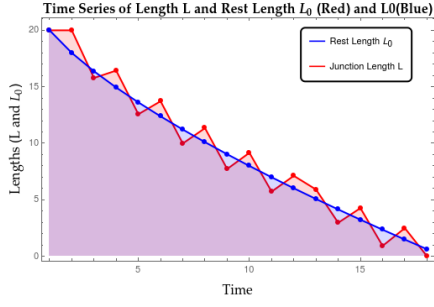
(b) $q_0 = 2.0$ and $q_s = 0.3$
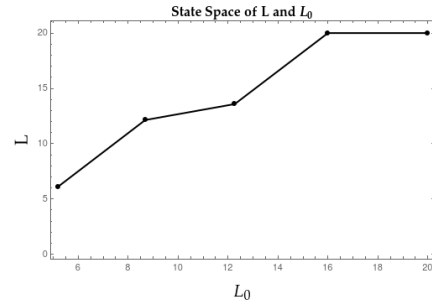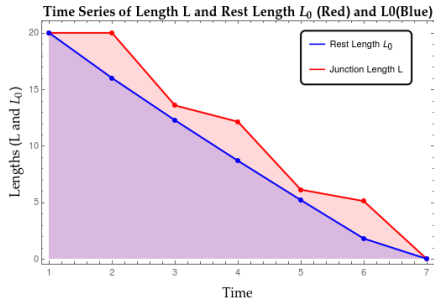
(c) $q_0 = 4.0$ and $q_s = 0.1$
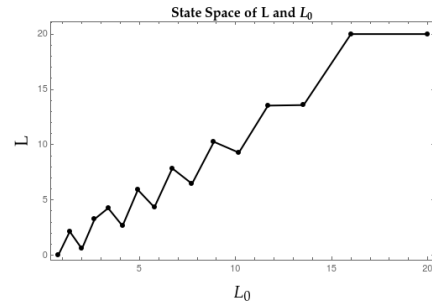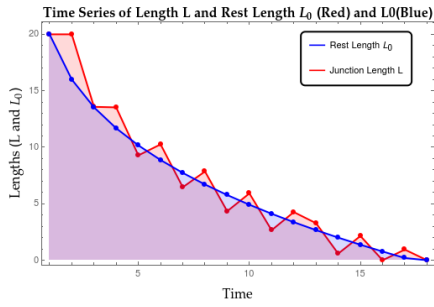
(d) $q_0 = 4.0$ and $q_s = 0.7$

Figure 4.13: Different L in dynamics with power law decay in Cadherin Density. The horizontal axis shows time and the vertical axis shows length (in a.u.). The rest length L_0 is marked in blue and the junction length L is marked in red. For a fixed value of q_0, changing the q_s changes the shape of the descent. A higher q_s exponent value leads to more accumulated backlash errors. As we increase q_0, it appears that the number of steps in the process decrease as a whole. ($\tau = 1.1$)

4.3.1 Phase Diagram of Accumulated Error for power law decay in E-Cad offset Q

Plotting the phase diagram, we notice the same three regimes, in markedly different regions from the exponential decay. This is despite the dynamics of the shrinkage "appearing" to be the same in both cases, at least qualitatively.
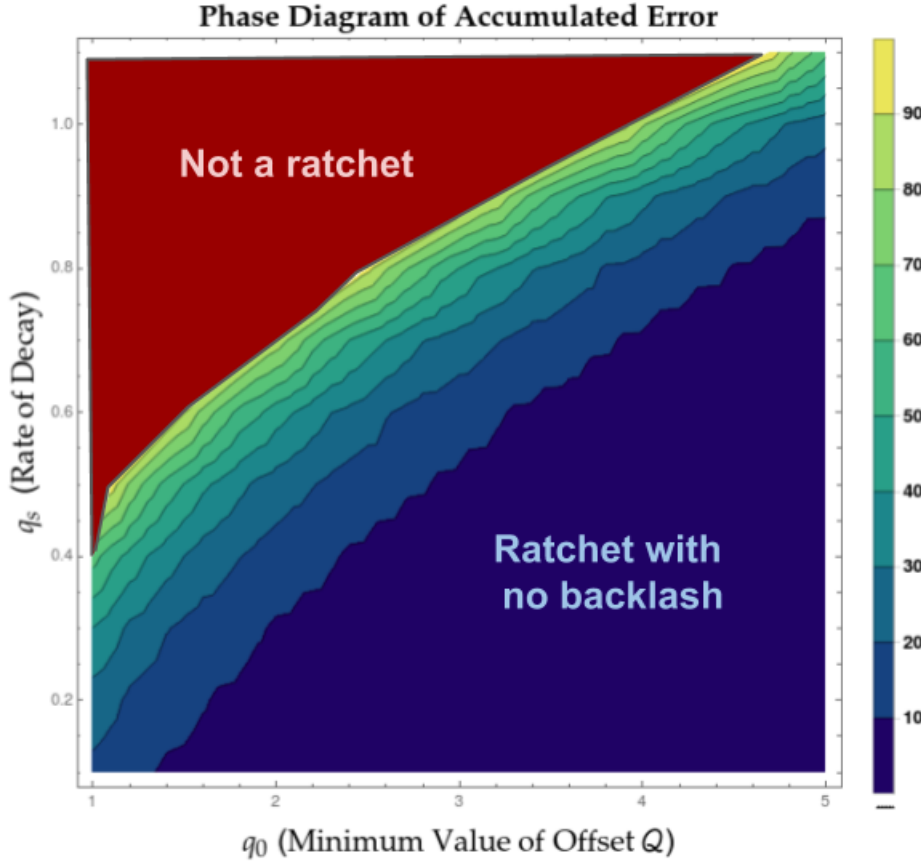
Figure 4.14: Phase Diagram for Accumulated Error in Q with power law decay. The horizontal axis has the minimum value of offset Q and the vertical axis has the power law exponent q_s. On the diagram itself, the total accumulated backlash error in color as a heat map (with the legend showing values). The regime marked in red is where the rest length crashes to zero in the very first step or never ratchets down and hence is disallowed, marked as not a ratchet. We also observe a dark blue area of a good ratchet with no backlash errors. Lower exponents with higher minimum values seems to give us better ratchet.

Chapter 5

Discussions and Future Directions

This work is an attempt to recast a microscopic model of cellular junction shrinkage into a more macroscopic, experimentally accessible model following the language of thermodynamics. We want to ask questions about reliability/robustness of a ratchet in this system and understand different models with increasing complexity. For each model, we set up the dynamics as discrete markov chains to create paths that the junction will follow. We attempt to understand what are the physically relevant parameters and how they affect the dynamics in the system and answer questions about parameters to quantify the goodness of a ratchet.

5.1   Discussion of results

We began with a simple model by constructing dynamics of the rest length L_0 to gain some intuition into the system. **We find that there must be offset in the rest length L_0 by some decrease in the E-Cadherin density in every Myosin cycle for a ratchet to exist.**. We also find that this model is not experimentally verifiable and hence we must construct a model independent of the exact L_0 dynamics. We build a second discrete time model that leads to the understanding that the rate of decay of rest length L_0 is crucial for the existence of a ratchet. **If the shrinkage in L_0 is very rapid, we get a bad ratchet with a lot of accumulated backlash error. A slow rate of shrinkage seems to yield a better ratchet** We also find an exponential decay is a more robust ratchet than a power law decay. Some more questions can be asked regarding the constructed paths.

1. How can we capture the noisy internal dynamics of the molecular players in a more coarse grained model?

2. How can we understand factors like entropy production in the system to find out bounds on shrinkage?

We look forward to answering these questions in the near future. We have also explored in greater detail the current models we have and adding more complexity with a E-Cad pulse time.

5.2 Choosing a protocol for time decay in offset

From the two protocols for time decay in the offset $Q(t)$, we would like to see if any of these protocols is a better choice for a good ratchet. One possible way to do this is by calculating work done for each path. A rough calculation for the same follows.

5.2.1 Choosing form of Q from work done calculations

We know the dynamic equations of the system. From this, the Hamiltonian of the system is calculated

$$\mathcal{H}(t) = (\frac{\tau}{2}(L(t) - L_0(t) + F^\alpha(t))^2) \tag{5.1}$$

Since our Hamiltonian is time dependant, we consider the thermodynamic work done on the system as[17]

$$\mathcal{W}_t(T) = \int_0^T dt \frac{\partial \mathcal{H}}{\partial t} \tag{5.2}$$

All the variables in the Hamiltonian equation are explicitly dependant only on time; the partial derivative simplifies out and in the discrete time limit, we can write the following (Setting any normalisation factors to 1 as we are only using it for comparison purposes):

$$\mathcal{W}_t = \sum_{i=0}^T \mathcal{H}_i \tag{5.3}$$

We calculate the work done for both the decay forms in the same regimes as the phase diagrams.
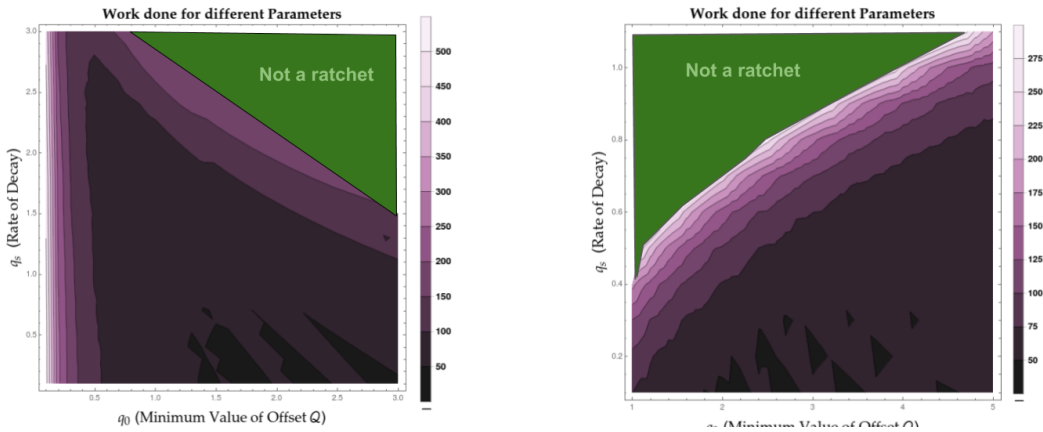
(a) Work Done for a Exponential Decay in $\mathcal{Q}$ **(b)** Work done for a power law decay in $\mathcal{Q}$

Figure 5.1: Work Done for each type of Decay in $\mathcal{Q}$. The horizontal axis has the minimum value of offset Q and the vertical axis has either **a)**the rate of decay in the exponential decay or **b)** the exponent of the power law in power law decay. On the diagram itself, the total accumulated backlash error in color as a heatmap (with the legend showing values)

For both the decay's, we can see some features in the regions of low work-done. This indicates that there are some paths that are more favorable than others, even in regions of zero backlash. To compare, we take the average of the work done over all the allowed paths considered. This value comes out to be 108.45 a.u for the exponential decay 85.467 a.u for the power law decays. It appears that a general power law form is a better ratchet.

5.2.2 A thermodynamic argument for the same

Our process is a time discrete process. We can approximate the steps in the system by assuming without too many caveats that the rest L_0 shrinks AFTER the length L has shrunk. This time delay can be taken to be infinitesimally small and there is no reason to believe that the processes happen simultaneously. We approximate that the process happens as follows:
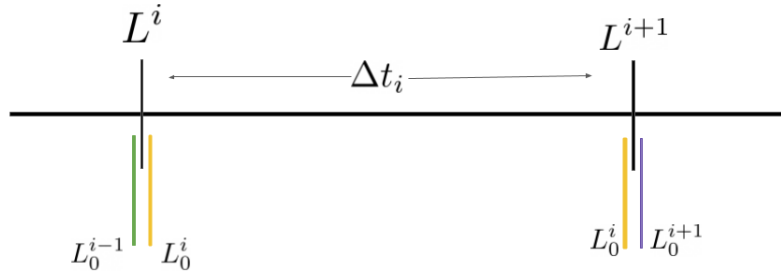
Figure 5.2: Changes in L and L_0 leading to microscopic reversibility

This lends microscopic reversibility to the shrinking process within a single interval and we can use the Jarjynzky equality[7]. In his seminal paper, Jarjynzky derived the inequality (which when combined with the convexity of the exponential function) yields

$$\Delta F \leq \bar{\mathcal{W}} \tag{5.4}$$

Here, the bar denotes indicates an average over all possible realizations that takes the system from the an equilibrium state to the non-equilibrium state. This is analogous to the work done, averaged over all paths, as calculated above. This provides us with an upper bound on the free energy available to the system.

Because of the microscopic reversibility, we can also use the Crooks Fluctuation Theorem[4] (with β normalised to 1)

$$\frac{P(A \to B)}{P(B \to A)} = e^{[\beta(\mathcal{W}_{A \to B} - \Delta F)} \tag{5.5}$$

We want to minimise the backward probability ($P(B \to A)$) to minimise backlash errors. The larger the argument in the exponential is, the smaller this probability will be. Since we have the upper bound of the free energy, we can calculate the lower bound on the argument and consequently, the upper bound on the backward probability.

Mathematical Calculations

For each form of decay,

1. We calculate upper bound of free energy $\bar{\mathcal{W}}$ for every move $i \rightarrow i+1$ from the ensemble average.

2. We choose the path with the least work done for each functional form of Q and calculate the backward probability for each individual move $i \rightarrow i+1$

3. Since each move in L is independent of the previous, the total backward probability is the sum of all individual backward probabilities.

Using this protocol, we can conclude that the general power law form is better than the exponential decay.
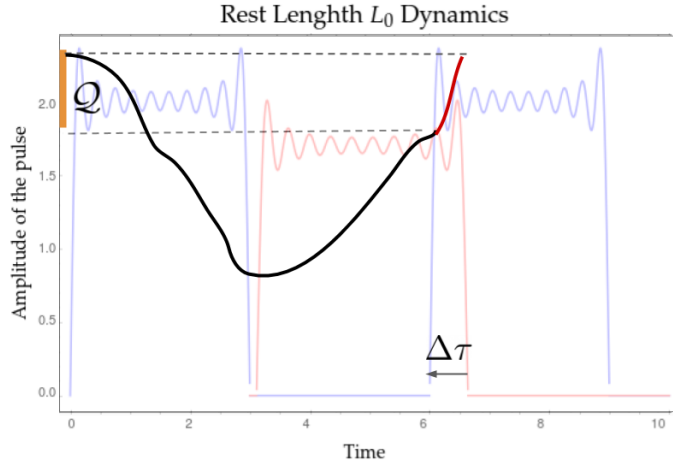
5.3 Model with the timescale of the Myosin and the E-Cadherin Pulse

We have so far looked at the force generator in the form of the Myosin pulse and the active force $F^\alpha(t)$. However, the interplay between the force generators and the force sensor E-Cadherin pulse can also be an interesting aspect to study. We know that the active force is impacted by the Myosin pulse. We also know that the density of E-Cadherin increases in pulses and opposes this shrinkage. We can assume that the rest length L_0 dynamics are controlled by the E-Cadherin pulse which pulses at a time scale of τ_c. We assume that the difference between the myosin and E-Cadherin time pulse is $\Delta\tau = \tau_m - \tau_c$. Assuming no interaction of any kind between the two pulses, we can visualise what the time scales could look like.
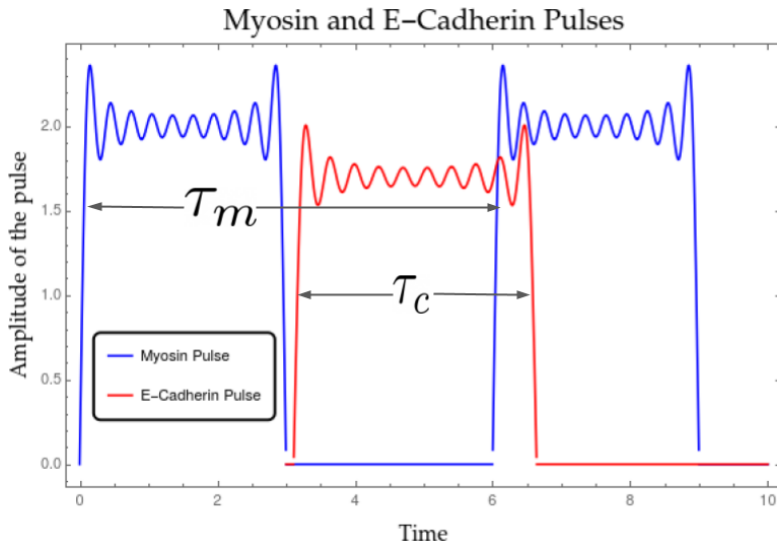
Figure 5.3: Form of Myosin and E-Cadherin pulse. The horizontal axis has time and the vertical axis has the amplitude of the pulses. The Myosin pulse (marked in blue) is on for a time period of τ_m. The E-Cadherin pulse with a different amplitude (marked in red, lower here for illustrative purposes) is on for a time period of τ_c. Since we know that the E-Cadherin pulse will oppose the shrinkage, it is a reasonable assumption that it is switched on when the Myosin pulse is switched off.

This affects the L_0 dynamics in the following way.

Figure 5.4: Form of L_0 with the Myosin and E-Cadherin pulse. The time has been marked on the horizontal axis. On the vertical axis, we have the amplitude of the pulse (to show the pulses in an illustrative manner) and the time difference $\Delta\tau$ has been marked. However, we care about the overlay of the rest length L_0, marked in Black. The red curve marks what dynamics of L_0 could be if the Myosin pulse had not reset the dynamics and the offset $\mathcal{Q}$ has been marked in Orange.

When the myosin pulse (blue) is on, the rest length shrinks. When the Cadherin pulse is switched on (Red), the shrinkage is opposed and the rest length starts to increase again. However, it does not increase to the previous value of L_0 as before the Cadherin Cycle can be completed, the next Myosin pulse kicks in the cycle is reset. If the rest length L_0 had been allowed to 'unshrink' for the entirety of the Cadherin time cycle τ_c, it would have reached the previous value (Shown in Red). This time difference $\Delta\tau$ is what leads to the offset $\mathcal{Q}$ in the dynamics. This $\Delta\tau$ is akin to a 'Phase Lag' between the two pulses. This can be visualised in a different space much better as:
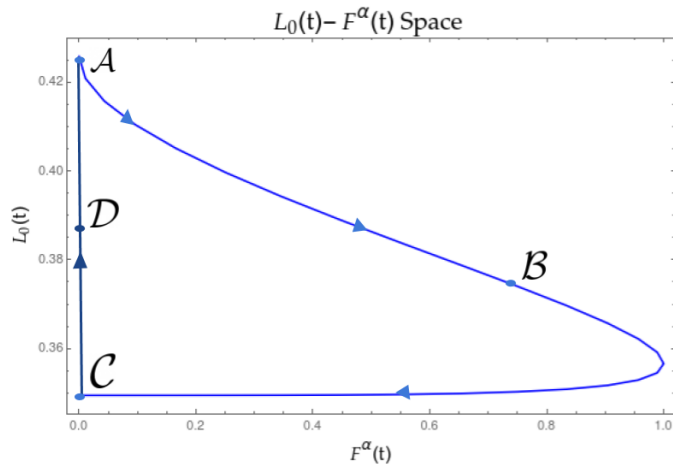
Figure 5.5: $L_0 - F^\alpha$ Space. The actual trajectory of L_0 is the curve $\mathcal{ABC}$ and that is when the Myosin Pulse and active force F^α reset it. The curve $\mathcal{CDA}$ is the trahectory that would be followed if the Myosin pulse had not reset till τ_c had completed its cycle.

This curve is paramterised by time. The segment ABC is the L_0 that is actually

followed in one myosin pulse time scale τ_m and the segment CDA is what would have happened if the next myosin pulse hadn't kicked in. The segment CDA happens over the timescale τ_c. We must note some things:

1. The following analysis will hold only for one myosin cycle and must be repeated separately for each myosin cycle.

2. The curve in Figure 5.5 is merely an illustrative example that has been created by writing down a simple fragmentation-aggregation model for the Cadherin Clusters. The actual shape of the curve is irrelevant to our analysis and will remain unknown as we do not have access to that level of microscopic detail.

Within this context, we can define our offset in L_0 to be the change in L_0 as we vary F^α over a time period τ_m (this would be represented by the segment CDA). For the ith myosin pulse, we can define

$$Q_i = \int_{(i-1)\tau_m}^{i\tau_m} L_0(t)\frac{\partial F^\alpha(t)}{\partial t}dt \qquad (5.6)$$

We can also write the line integral on the simply connected, closed curve $ABCD$ and using the Cauchy Integral Theorem:

$$\underbrace{\int_{(i-1)\tau_m}^{i\tau_m} L_0(t)\frac{\partial F^\alpha(t)}{\partial t}dt}_{ABC} + \underbrace{\int_{i\tau_m}^{i\tau_m+\tau_c} L_0(t)\frac{\partial F^\alpha(t)}{\partial t}dt}_{CDA} = 0 \qquad (5.7)$$

(We are assuming there are no poles in the area under the curve, which seems reasonable as the equations never blow up to infinity in the real world dynamics). Hence, this equality holds. Using Equation 5.6, we get

$$Q_i + \underbrace{\int_{i\tau_m}^{i\tau_m+\tau_c} L_0(t)\frac{\partial F^\alpha(t)}{\partial t}dt}_{CDA} = 0 \qquad (5.8)$$

For ease of writing, without loss of generality, we can set $i = 1$ which is the first move in the shrinkage of the junction. We can Taylor expand the second term of the equation around $i\tau_c$ to give us a form for Q_i as

$$Q_i + \int_{\tau_m}^{\tau_m+\tau_c} L_0(\tau_c)\frac{\partial F^\alpha(t)}{\partial t}\Big|_{\tau_c}dt + \int_{\tau_m}^{\tau_m+\tau_c} \frac{\tau_c}{2}\Big[L_0'(\tau_c)\frac{\partial F^\alpha(t)}{\partial t}\Big|_{\tau_c} + L_0(\tau_c)\frac{\partial^2 F^\alpha(t)}{\partial t^2}\Big|_{\tau_c}\Big]dt + O(\tau_c^2) = 0 \qquad (5.9)$$

The first term in the second integral is a product of two derivatives. Since we have seen that the rest length cannot shrink very rapidly, these rates of change values will be very small and this term can be neglected. Solving the simple linear integrals, we get a form for each Q_i at a time scale of τ_m as a function of τ_c

$$Q_i + \tau_c L_0(\tau_c)\frac{\partial F^\alpha(t)}{\partial t}\Big|_{\tau_c} + \frac{\tau_c^2}{2}L_0(\tau_c)\frac{\partial^2 F^\alpha(t)}{\partial t^2}\Big|_{\tau_c} = 0 \qquad (5.10)$$

This can now be solved by either substituting a constant value for Q_i like was assumed in the first model, or with a time dependant quantity like in the second model.

Bibliography

[1]   R. Dean Astumian. "Thermodynamics and Kinetics of a Brownian Motor". In: *Science* 276.5314 (1997), pp. 917–922. ISSN: 0036-8075. DOI: `10.1126/science.276.5314.917`. eprint: `https://science.sciencemag.org/content/276/5314/917.full.pdf`. URL: `https://science.sciencemag.org/content/276/5314/917`.

[2]   Deb Sankar Bannerjee. "Active hydrodynamics of actomyosin elastomer with turnover during tissue remodeling". PhD thesis. Jawaharlal Nehru University, 2018.

[3]   MIT Open CourseWare. *1.2.4 The Forward Euler Method*.

[4]   Gavin E. Crooks. "Entropy production fluctuation theorem and the nonequilibrium work relation for free energy differences". In: *Phys. Rev. E* 60 (3 Sept. 1999), pp. 2721–2726. DOI: `10.1103/PhysRevE.60.2721`. URL: `https://link.aps.org/doi/10.1103/PhysRevE.60.2721`.

[5]   Kai Dierkes et al. "Spontaneous Oscillations of Elastic Contractile Materials with Turnover". In: *Phys. Rev. Lett.* 113 (14 Oct. 2014), p. 148102. DOI: `10.1103/PhysRevLett.113.148102`. URL: `https://link.aps.org/doi/10.1103/PhysRevLett.113.148102`.

[6]   Zahra Erami et al. "There are four dynamically and functionally distinct populations of E-cadherin in cell junctions". In: *Biology Open* 4.11 (2015), pp. 1481–1489. DOI: `10.1242/bio.014159`. eprint: `https://bio.biologists.org/content/4/11/1481.full.pdf`. URL: `https://bio.biologists.org/content/4/11/1481`.

[7]   C. Jarzynski. "Nonequilibrium Equality for Free Energy Differences". In: *Physical Review Letters* 78.14 (Apr. 1997), pp. 2690–2693. DOI: `10.1103/physrevlett.78.2690`. URL: `https://doi.org/10.1103/physrevlett.78.2690`.

[8]   Deqing Kong, Fred Wolf, and Jörg Großhans. "Forces directing germ-band extension in Drosophila embryos". In: *Mechanisms of Development* 144 (2017). Roles of physical forces in development, pp. 11–22. ISSN: 0925-4773. DOI: `https://doi.org/10.1016/j.mod.2016.12.001`. URL: `http://www.sciencedirect.com/science/article/pii/S0925477316300971`.

[9]   Bryan Lau et al. "An introduction to ratchets in chemistry and biology". In: *Mater. Horiz.* 4 (3 2017), pp. 310–318. DOI: `10.1039/C7MH00062F`.

[10] Deb Shankar Bannerjee; Kabir Husain; Girish Kale; Thomas Lecuit and Madan Rao. "Medial and junctional myosin work in tandem to ratchet junctional shrinkage". In: *unpublished* (). manuscript under preparation.

[11] Peter Novick. "Regulation of membrane traffic by Rab GEF and GAP cascades". In: *Small GTPases* 7 (4 2016), pp. 252–256. DOI: `1080/21541248.2016.1213781`.

[12] Anup Padmanabhan, Hui Ting Ong, and Ronen Zaidel-Bar. "Non-junctional E-Cadherin Clusters Regulate the Actomyosin Cortex in the C. elegans Zygote". In: *Current Biology* 27.1 (2017), pp. 103–112. ISSN: 0960-9822. DOI: `https://doi.org/10.1016/j.cub.2016.10.032`. URL: `http://www.sciencedirect.com/science/article/pii/S0960982216312581`.

[13] Matteo Rauzi, Pierre-François Lenne, and Thomas Lecuit. "Planar polarized actomyosin contractile flows control epithelial junction remodelling". In: *Nature* 468.7327 (2010), pp. 1110–1114. ISSN: 1476-4687. DOI: `10.1038/nature09566`. URL: `https://doi.org/10.1038/nature09566`.

[14] Peter Reimann. "Brownian motors: noisy transport far from equilibrium". In: *Physics Reports* 361.2-4 (Apr. 2002), pp. 57–265. ISSN: 0370-1573. DOI: `10.1016/s0370-1573(01)00081-3`. URL: `http://dx.doi.org/10.1016/S0370-1573(01)00081-3`.

[15] Udo Seifert. "Stochastic thermodynamics, fluctuation theorems and molecular machines". In: *Reports on Progress in Physics* 75.12 (Nov. 2012), p. 126001. ISSN: 1361-6633. DOI: `10.1088/0034-4885/75/12/126001`. URL: `http://dx.doi.org/10.1088/0034-4885/75/12/126001`.

[16] Ding Zemin and Fengrui Sun. "Optimum performance analysis of Feynman's engine as cold and hot ratchets". In: *Journal of Non Equilibrium Thermodynamics* 36 (June 2011), pp. 155–177. DOI: `10.1515/jnetdy.2011.011`.

[17] Eric N. Zimanyi and Robert J. Silbey. "The work-Hamiltonian connection and the usefulness of the Jarzynski equality for free energy calculations". In: *The Journal of Chemical Physics* 130.17 (May 2009), p. 171102. DOI: `10.1063/1.3132747`. URL: `https://doi.org/10.1063/1.3132747`.